Title
Critical examination of ultrasonic transducer characteristics and calibration methods

Journal
Research in Nondestructive Evaluation, 30(1)

ISSN
0934-9847

Author
Ono, Kanji

Publication Date
2019-01-02

DOI
10.1080/09349847.2017.1375585

Peer reviewed

Critical Examination of Ultrasonic Transducer Characteristics and Calibration Methods

Kanji Ono
Department of Materials Science and Engineering, University of California, Los Angeles (UCLA),
Los Angeles, CA 90095, USA; ono@ucla.edu

Abstract

This study systematically determined the transmission and receiving sensitivities of over twenty transducers. Four types of sensitivities were evaluated for both transmission and receiving sensitivities. These are found to be different from each other and the reversibility or reciprocity conditions exist only in exceptional cases. Using their observed behavior as the basis, we critically examined the calibration methods developed to characterize them, including those based on laser interferometry and the acoustic reciprocity principle. Serious flaws in some of the reciprocity methods are uncovered, which can be rectified by using Hill-Adams method. Four procedures emerged as workable calibration methods for contact ultrasonic and acoustic emission transducers. However, current experimental uncertainties limit the upper frequency to 2 MHz.

Keywords

Ultrasonic transducer, acoustic emission sensor, calibration methods, reciprocity, laser interferometry

1. Introduction

In ultrasonic testing (UT) and acoustic emission (AE) testing, transducers and sensors are key components in the measurement chains and their characteristics are needed in the analysis of test results. Methods of their characterization have been developed over the years and some international standards have been formulated. Unlike hydrophone calibration, however, commonly accepted standard calibration procedures have not been developed in both UT and AE fields except for limited cases. One such exception is ISO12713/ASTM E1106 for surface wave calibration method for contact AE sensors [1]. Actually, water-immersible reference sensors can be calibrated in verified hydrostatic pressure fields, maintained at some standards laboratory to 20 MHz and these can be used for secondary calibration procedures [2]. This has been used sparingly, perhaps because of the cost of such calibration, and no standard practice guidelines have been written.

Another approach is to utilize the so-called reciprocity calibration methods, originally developed for hydrophone calibration [3-9]. This has been considered as procedures that require no physical measurement of acoustic pressure or displacement (or velocity) under the assumption that all transducers and sensors operate in reciprocal manner. The transmission and receiving sensitivities are defined S and M, in terms of transfer functions. Further, S is defined for current input in terms of acoustic pressure at a reference distance from the

transmitter, thus including the transmission transfer function, X. M is in terms of velocity input and voltage output. For a set of mutually reciprocal transducers, MacLean [3] set their ratio, $(M/S)_i = (M/S)_j = \dots$, to be identical (to be referred to as MacLean's reciprocity condition) and to depend only on geometrical conditions dictating sound transmission. This ratio is usually called reciprocity parameter (or factor). Here, we can separately denote the transmission sensitivity of a transducer proper as S° with $S = S^\circ X$. When the part of wave transmission through a coupling medium is separated as X, the ratio of M and S° becomes X. This X factor can be geometry and frequency dependent, containing no effect from the transducer. Hill and Adams [10] introduced this approach as well as Schmerr and coworkers more recently [8]. Schmerr [9] further defined the condition of reciprocity for a single transducer to be an equality of M and S°, or $M = S^\circ$ (to be referred to as Schmerr's reciprocity condition). When the X factor that only includes wave transmission effects is separated, this appears to be a logical development. The third reciprocity condition was given by McMillan [11]. This is based on linear, passive network representation of electromechanical systems using the force-voltage and velocity-current correlations. Hence, the network must not be dissipative. McMillan's reciprocity condition is the equality of two transfer impedances. When he applies this to the case of piezoelectric transducers, this leads to the absence of real component in the input or output impedance and to 90° out of phase condition for the input current and force output. The latter is generally found in simple, non-dissipative piezoelectric and capacitive transducers, imparting them reciprocal behavior. However, his basic assumption of non-dissipative systems poses a severe restriction in dealing with typically damped modern piezoelectric transducers. Thus, we have three theoretical conditions for the examination of the reciprocity of transducers. These will be utilized in combination with experimentally obtained transducer characteristics in the present study. More references and discussion on the reciprocity calibration methods were given in our previous work [12].

In a variation of reciprocity calibration methods, three transducers, t1, t2 and t3, are used in a sequential (1-2-3) combination as transmitter and receiver (t1>t2, t2>t3 and t3>t1), producing output voltages E_{12}, E_{23}, and E_{31}, corresponding to the driving input current, I_{12}, I_{23}, and I_{31}. When the signal direction is reversed, output voltages E_{21}, E_{32}, and E_{13} are obtained and if these are identical to the corresponding output, or $E_{ij}/I_{ij} = E_{ji}/I_{ji}$, the transducer pair is reversible and MacLean [3] used this as proof of transducer reciprocity.

Starting with MacLean [3], $E_{12}/I_{12} = E_{21}/I_{21}$ is interpreted to mean $S_1 M_2 = S_2 M_1$. MacLean, then, defined a ratio, $M_1/S_1 = M_2/S_2$. When we know at least one of the four parameters, we can use the reversibility condition of $E_{12}/I_{12} = E_{21}/I_{21}$ to generate the M/S ratios. However, these M and S values are unknowns at this stage. A unique M/S ratio cannot be obtained from the M-S product unless M and S° are equal. When $M \neq S^\circ$, $M/S^\circ X = M/S$ and choices for this ratio on the basis of the reversibility becomes infinite. It is clear that we cannot obtain the reciprocity equation of $M_1/S_1 = M_2/S_2$, starting from the reversibility equation of $E_{12}/I_{12} = E_{21}/I_{21}$. When we have separate M and S, we can get to the reversibility equation, but we cannot extract current part. This logical gap seems to persist in the literature even today.

When the reversibility conditions of $E_{ij}/I_{ij} = E_{ji}/I_{ji}$ exist, we can use the sequential transmission and receiving set-up to obtain output voltages E_{12}, E_{23}, and E_{31}. Separating the transmission transfer function X from S, we can determine the products of the transmission and receiving sensitivities from the output voltages, E_{ij}. Using the separated X function (X = 1 can be used for the commonly used face-to-face coupling of contact transducers), it is easy to show that

$$M_i S^\circ_i = E_{ji} E_{ik} I_{jk} / E_{jk} I_{ji} I_{ik} X \qquad (1)$$

(with i, j, and k taking 1 to 3). When $M_i = S^\circ_i$, we have three values for the three reversibility equations. If we have one of the six unknowns (S°_i and M_i) or one of three ratios (as there is no a priori reason for assuming the ratio being invariant), we can determine all of the sensitivities. It appears that the M-S° product is useful and adequate in the case of pulse-echo UT. In fact, transducer manufacturers typically provide the echo waveform (or E_{ii}) on a standard pulser-receiver and its power spectrum for UT transducers (or the product of M and S°).

In the above formulation of reversibility, conventional choice of variables is used. However, another set of variables also leads to the equivalent reversibility condition. We can utilize driving voltage input and normal displacement output for a transmitter and displacement input and voltage output for a receiver. The input voltage and current are related by the transducer impedance, while the velocity is the time-derivative of displacement. Thus, when the impedance of two transducers are identical, the voltage and current ratios are equal to each other. As will be shown later, we can obtain equations similar to eqn (1) in terms of voltage input and displacement variables. Some transducer pairs exhibit reversible behavior with this alternate set of transducer sensitivities.

Hill and Adams [10] modified the second variation of reciprocity calibration methods without requiring the equality of S° and M. Here, the transmitter-receiver combinations of (t1>t2, t1>t3 and t3>t2 or 1-1-3 combination) is used, but no reversibility conditions are required. However, the ratio of the receiving and transmission sensitivities of transducer 3, M_3/S°_3, must be known. They derived an expression giving the receiving sensitivity of transducer 2. This is Hill-Adams equation and is given as

$$M_2 = [(E_{12} E_{32} / E_{13} I_3 X)(M_3/S^\circ_3)]^{0.5}, \qquad (2)$$

where X is the transmission transfer function for the t3>t2 path and I_3 is the input current to transmitter 3. (Typographical errors in the original equation are corrected.) Here, X for the path 1>2 and 1>3 are assumed equal and factored out.

Many studies of reciprocity calibration methods in the UT and AE fields skipped detailed reporting of reciprocity parameters and their experimental validation appears missing even though this part often is the central effort in air-borne acoustic transducers. Schmerr and coworkers [8, 9] have presented extensive modeling studies of pulse-echo and through transmission ultrasonics, but the validation of sensitivity parameters with physical measurements of particle velocity or displacement was not included. Hatano and coworkers

[13, 14] applied reciprocity calibration methods to contact AE transducers, but their reciprocity parameters only included the wave transmission effects. As noted earlier, this leads to the equality of M and S˚, but no experimental confirmation was part of their work. Goujon and Baboux [15] and Keprt and Benes [16] similarly showed calibration results of reciprocity calibration methods, but provided no details of their calibration methods, including reciprocity parameters.

Recently, we have used laser interferometry to characterize the transmission sensitivities of UT transducers in order to develop the basis for AE sensor calibration [12]. While some consistent results have been obtained, further improvements are desirable as free transducer faces on some produce spurious vibration, different from front-loaded transmission cases. Toward that goal, a comparison with other available methods, especially with the reciprocity calibration methods, may lead to refinement, but existing documents are ambiguous and most lack adequate independent validation. In the present study, we use the receiving and transmission sensitivities of nine transducers we have determined using the laser-based methods reported earlier. These are then combined to evaluate if the reversibility conditions exist among various pairs of these calibrated transducers. If this is the case, this adds another tool for the validation of the methods based on laser interferometry. We also use sets of identical transducers toward the same goal as different transducer designs/models often led to the absence of reversibility when we used voltage-based sensitivities. One of the sets exhibited full reversibility and this set was used to examine various calibration approach for validation. Some researchers also contend that transducer calibration is impossible without driving current measurements [13, 14]. We have compared static and dynamic impedance measurements and show that either voltage or current measurements lead to consistent calibration outcomes. It is also found that the current term in Hill-Adams equation is not required, eliminating the needs for current probe measurement entirely.

From comparison of calibration methods, we find that the direct/indirect methods based on displacement measurement and Hill-Adams method, which is a variation of the reciprocity calibration methods, using a reference transducer of known sensitivity ratio, provide consistent and verifiable outcomes. It is also discovered that one common variation of the reciprocity calibration methods contains a fatal flaw of including an unknown parameter in the sensitivity equation, making it utterly useless.

2. Experimental Methods and Results

2.1 Basic procedures

The basic information we utilize to characterize the receiving and transmission sensitivities of transducers is the normal displacement waveform observed on the face of a transducer, driven by a short mono-polar pulse. It is a negative-going step-down pulse (for 50-Ω load, 80 ns to the peak at 200 V) decaying to zero in a few μs. The displacement outputs of the transducers and experimental details were reported earlier [12]. Transducers examined were Olympus V101 (0.5), V103 (1), V104 (2.25), V107 (5), V111 (10), V189 (0.5), V192 (1) and V195 (2.25) designed

for ultrasonics as well as Physical Acoustics R15 resonant AE sensors. Other transducers (AET FC500 (2.25), PAC F30 (0.3), R6a (0.06) and Fuji REF-VL (0.3)) were also included in this study. Transducer details are given in Appendix Table A1. The nominal resonant frequency of each transducer in MHz is given in parentheses following its designation unless it becomes repetitive.

Two laser interferometry examples are shown in Fig. 1a for Olympus V107 (5) and V111 (10) UT transducers, together with the driving pulse waveforms (Fig. 1b). These were not included in our previous study. The peak values are 6 to 9 nm, with a decaying tail lasting over 10 μs. However, the main pulse has <2 μs duration. Their FFT magnitude spectra are given in Fig. 2, showing gradually decaying curves with more noise above 2.5-3 MHz, and becoming much noisier above 5 MHz (not shown). Three more curves from previous study are also provided. Smaller transducer (V104 (2.25)) develops low frequency oscillations, while larger V192 (1) and V195 (2.25) give smooth spectra below 2 MHz. Both V104 and V195 (2.25 MHz, 38-mm) also extend smooth transmission output to 4 MHz. Note that higher performance pulsers are available commercially, but these were not available for this study. In addition, such pulsers are typically many times larger than the present pulser that has only a ½-liter volume and is easy to transport to the laser interferometry facility, located at Aoyama Gakuin University, Sagamihara, Japan.

Using the same pulser set-up, we determined the driving current for these transducers. One example is shown in Fig. 3 for PAC R15. The current pulse peaks at 0.98 A and the initial half pulse is similar in shape to dV/dt of the voltage pulse shown in green, indicative of capacitive response. The voltage pulse has a peak at -194 V. The current spectra for three transducers (Fig. 4) rise sharply at low frequencies, but flatten above 200-300 kHz. The peak current ranges from 0.95 A for V103 to 4.4 A for V104. The highest observed was for V195, which peaked at 8.73 A. The current pulse was measured using a Hioki 3273 current probe (50 MHz, 10-A capacity) while high voltage pulse was measured using B&K 1/100-probe. Another current probe (constructed in-house) was also utilized giving matching impedance results within 0.5 dB, but their responses are treated separately from Hioki results. Signals were recorded using PicoScope 3405A at 2 ns sampling interval with 20 MHz low-pass filter. For the in-house current probes, sinewaves were also used as input and the rms voltage values were compared. As expected, the probe sensitivity decreased at low frequencies below 200 kHz. Separately, the displacement output of the transducer with pulse input was measured using Thales SH140 laser interferometer with 20 MHz bandwidth.

2.2 Electrical impedance

Electrical impedance is extended from electrical resistance and has a complex value. This is widely used in eddy-current testing and is represented by $Z = R + i X$ where real resistance R (in the x direction in an impedance diagram), $i^2 = -1$, and imaginary component X (in the y direction). An inductor of L henry has $X = +2\pi fL$ (in ohms with frequency f in Hz) and a capacitance C farad has $X = -(1/2\pi fC)$ (also in ohms). In terms of Z, a piezoelectric transducer primarily behaves as a capacitor and its frequency dependence is inversely proportional to frequency. For example, a V103 (1) transducer has C = 432 pF and Z = 737 Ω at 0.5 MHz (or 57.3

dB in reference to 0 dB at 1 Ω. Also for an R15 (0.15) transducer, C = 188 pF and Z = 1.69 kΩ (64.6 dB) also at 0.5 MHz. In a Z – f plot (Z in dB and *f* in logarithmic scale), most piezoelectric transducers show nearly straight lines with the slope of –1. Z of a transducer can be measured by passing ac signals and by dividing applied voltage by (complex) current flowing through it. The applied ac signal can by a broadband pulse or sinewave wavelets of varying frequency. Here, both methods are utilized.

Using a pulse method, we can obtain the input electrical impedance (Z) of the transducers from the driving voltage and current signals. Their spectra are given in Fig. 5. Typically, these show different curves for various transducers but most showing the capacitive behavior with Z inversely proportional to frequency. For R15 (green), Z value ranged from ~16 kΩ to ~120 Ω decreasing with frequency. At 0.5 MHz, Z was 62.7 dB, within 2 dB of the value calculated above from a capacitance measurement made at 200 kHz. For V195 (blue), Z has a maximum near 2.7 MHz. Z increases initially from ~1.6 Ω to 55 Ω, then decreasing above 2.7 MHz. Most others showed a decreasing trend of Z slightly steeper than R15, but with less oscillations. In some cases, they coincide. For V101 (blue) and V111 (purple dash), the Z curves agree well. Another pair that matches well is that of V189 (purple) and V192 (dark red). Z for V104 (dash-dot purple) follows closely to the pair of V189-192, but is slightly higher above 2 MHz. These are near the lowest except for V195. The highest Z is shown by R15 resonant AE sensor (top green curve), followed by V103 (red). At 0.5 MHz, Z was 57.0 dB, within 0.3 dB of the value calculated above. R15 (green) curve below 0.5 MHz exhibits some oscillations due to low frequency resonances.

Z for V195 has an inductive component, indicating 1.1 µH at 200 kHz, when measured using an LCR meter (LCR45, Peak Electronic Design). In addition, it shows dc resistance of 0.80 Ω, which makes V195 non-reciprocal according to McMillan's condition. These Z values are 5-6 dB lower than the curve for V195 in Fig. 5. Another set of Z measurements for V195 used HP 4800A vector impedance meter over 9 to 550 kHz. Z was at 1.0 Ω at 9 kHz and increased gradually to 4.6 Ω at 550 kHz. The static Z values, measured using continuous sinewaves, matched well with the results from dynamic tests with pulses (shown in blue dash curves in Fig. 5) between 75 kHz to 150 kHz, but were 3 dB lower >250 kHz. Most notably, the phase angle started at +5˚, increasing to +71.3˚. That is, this V195 is resistive below 30 kHz, becoming increasingly inductive. This clearly indicates that V195 is non-reciprocal because the McMillan reciprocity condition [11] is violated. Furthermore, not all UT transducers are reciprocal, even though they are piezoelectric since some of them are designed with damping to broaden the bandwidth. Again, the McMillan reciprocity condition is not satisfied.

Z values for V189 and V192 with HP4800A agree with the results of dynamic measurements to better than 2 dB. The phase angle is –70˚to –80˚, indicative of nearly capacitive response, but it approaches –90˚ only for V189 below 30 kHz. Thus, these two mostly fail the McMillan condition of 90˚ out of phase.

For three of the transducers (R15, V101 and V103), we determined Z using a potentiostat from 20 kHz to 1 MHz and reported the results previously [12]. These results are compared with Z from the present pulse measurements in Fig. 6. Overall trends and values match well. For R15,

low frequency oscillations were observed in the static case with more details, while Z from the dynamic measurement is smoothed out. In the case of V101 and V103, no low frequency oscillations were found in both measurements and agreement is excellent at >20 kHz. The phase angles for these tests are mostly below –85˚, indicating the capacitive responses, except at R15 resonances. When the response is capacitive, the McMillan reciprocity condition [11] is met, but is violated otherwise. This finding implies the lack of reciprocity at sensor resonances.

The above results on the input impedance of transducers have shown generally capacitive behavior, except for resonating type, such as R15, and for one with special design, such as V195. Thus, the observed Z behavior for most transducers tested does not violate the McMillan reciprocity condition by itself. The differences between pulse and continuous wave Z measurements are as expected since various resonances are readily excited by longer excitation times in the latter method. In addition, the pulse method is more sensitive to noise since it relies on broadband signals in both voltage and current measurements.

Another impedance parameter of interest is the output electrical impedance. This can be measured by applying mechanical impulse on the transducer front face (by another transducer driven by a pulser) and by measuring the output voltage and short-circuit current. In our case, we used 1-Ω resistor and measured drop-off voltage for current. Both high and low frequency transmitters were used to provide as much mechanical excitation as short-circuit current is down to tens of mA, especially for low frequency transducers like R15. It was also desired to avoid using an amplifier.

Representative results are shown as solid curves in Fig. 7 by plotting along with input electrical impedance (dashed curves). Except for the cases of a R15 sensor at resonances and V195 below 100 kHz, both values of Z match reasonably well. The difference is typically 3 dB or less over 30 kHz to 1 MHz. It is unclear how the large discrepancies develop in V195 at frequencies below 100 kHz, but this is also the range where its receiving sensitivity rises while the transmission sensitivity exhibits no large changes. Thus, we can conclude that the input and output electrical impedance of these transducers agree with each other except where resonant behavior is present.

In normal ultrasonic testing, a transducer is used within a full-width at half-maximum (FWHM) band centering at its nominal resonant frequency. That is, the bandwidth is defined at –6 dB points from the maximum. For example, broadband 2.25-MHz transducers like V104 and V195 are used over 1 to 4 MHz based on their pulse-echo spectra. These have transmission and receiving sensitivities beyond such commonly used FWHM ranges, as reported previously [12]. When these are used as reference transducers, the useable bandwidth can be extended to –20 dB from the peak value without seriously compromising the accuracy. Actually, the methods used in this work can reproduce sensitivity data with consistency even at –40 dB down, as will be shown later. The off-resonance behavior of most AE sensors that rely on resonating sensing elements is of low practical value because it is common to further limit the bandwidth in the sensing electronics. However, some sensors show a peak sensitivity at frequency not recommended by manufacturers and it is necessary to be aware of such a behavior in their use.

2.3 Transmission sensitivities

Using a laser interferometer, we determined the displacement output, T (in nm), from transducers driven by pulse input. Because of differences in the transducer impedance, actual voltage and current input vary with a particular transducer even though a single pulser is operated at the same condition. The levels of the displacement output for all the transducers are similar to those shown in Fig. 2. Most of them were reported previously. Except for V195 (2.25 - purple), a general trend is observed where the values of T decrease with frequency, starting from ~100 dB at 22 kHz, dropping to 93-100 dB at 200 kHz and to 60-80 dB at 2 MHz. Here, 0 dB corresponds to 1-nm displacement. V195 shows similar T values of 72-74 dB to 1 MHz, peaking at 1.7 MHz then decreasing above. As expected, R15 shows peaks at its resonant frequencies, ~130 kHz and a few more, resembling its input Z behavior in Fig. 7. Here, it should be noted that the FFT magnitude output from Noesis we used in this study is higher by 20 log (N), where N is the length of input file in comparison to some other FFT routines. We use N = 256 k and the difference is 108.37 dB. Some of the transducers develop spurious oscillations and corrections were made as discussed in the previous study [12]. Mutually consistent displacement transmission sensitivities for all the transducers have been determined. Among the laser data in Fig. 2, for example, V107 (5) shows higher output below 1 MHz and actual face-loaded output is up to 5 dB less below the laser data (corrected data is shown in Fig. 8). On the other hand, some, like V104 (2.25) and V192 (1), required no such correction.

These displacement transmission spectra can be converted to those with output in the time-derivative of displacement or particle velocity by multiplying $2\pi f$. By further subtracting 180 dB, the reference becomes 0 dB at 1 (m/s). When we subtract corresponding power spectrum for voltage- or current-input pulse from these transmission spectra in displacement or in velocity, we can remove the effects of driving high-voltage pulse and determine the transmission sensitivities in displacement or in velocity in reference to unit voltage input or current input. That is, there are four different types of transmission sensitivity for a given transducer. The transmission sensitivities in displacement in reference to voltage input was denoted as t_i for the i-th transducer previously [12]. Here, we use subscript to indicate voltage (v) or current (c) and use a superscript (n) to designate transducer n. Thus, for transducer n, we have transmission sensitivities of

$t_v^{(n)}$	displacement in reference to voltage-input (nm/V)	red curve
$t_c^{(n)}$	displacement in reference to current-input (nm/A)	green curve
$t'_v{}^{(n)}$	velocity in reference to voltage-input (m/sV)	red dotted curve
$t'_c{}^{(n)}$	velocity in reference to current-input (m/sA)	green dotted curve

In Fig. 8, four transmission sensitivities for V107 (5 MHz-12.7 mm) are plotted as an example. All other UT transducers tested behave similarly. The top red dashed curve is voltage spectrum of the driving pulse (V_{in}) while the green dashed curve is the input current spectrum (I_{in}). Solid blue curve (usually between these two pulse spectra) is the displacement spectrum (T). Here, the displacement-voltage and velocity-current spectra (t_v and t'_c) are close to each other above

200 kHz. These are 3-4 dB apart to 2.5 MHz and the differences shrink to 1 dB at higher frequencies. However, other spectra have no resemblance to each other. Although this transducer has the nominal center frequency of 5 MHz, the data beyond 6 MHz became noisy and was cut off at 8 MHz. The resonance peak was at 4.2 MHz in terms of the displacement-voltage spectrum and FWHM bandwidth was from 3.2 to 5.2 MHz, but the overall behavior was of broadband, varying ±5 dB from 0 to 6 MHz.

Figure 9 gives an example of a resonant AE sensor (PAC R15 (0.15)), giving entirely different characteristics. Spectral curves (with the same color codes) have many peaks and valleys from resonances and anti-resonances. All the transmission spectra are full of sharp oscillations beyond the primary resonance zone of 100-200 kHz from higher harmonics. Above 200 kHz, the displacement-voltage and velocity-current spectra are parallel to each other as was the case in V107 (5). These are about 15 dB apart to 2.5 MHz. This similarity of the displacement-voltage and velocity-current spectra is common in most UT transducers. In V101 (0.5) and V111 (10), the curves match to better than 1 dB (>100 kHz), while in others (except V195 (2.25)) the differences are about 6 dB. However, V195 shows completely different spectra, reflecting different impedance characteristics from all others (cf. Fig. 5).

In examining the transmission behavior of transducers, we also need to compare various waveforms, as shown in Fig. 10 for V101 (0.5), V104 (2.25) and V111 (10). These include displacement output (T), its time-derivative or velocity (dT/dt = T'), input voltage (V_{in}), its time-derivative (dV_{in}/dt) and input current (I_{in}). Three examples are given in Fig. 10 (with T in purple, T' in purple dash, V_{in} in blue, dV_{in}/dt in green and I_{in} in red). In all three, curves for dV_{in}/dt and input current have similar behavior, especially at the initial stage. This represents the capacitive response. For higher frequency transducers (V104 and V111), curves for V_{in} and T follow the same trend. However, T for V104 rises more slowly than V_{in} and the V_{in} and T curves do not match after reaching the initial maximum with T's showing some oscillations. V107 (5 MHz) transducer responded with a behavior between these two (2.25 and 10 MHz). The low frequency V101 (0.5 MHz) has completely different V_{in} and T curves. On the high frequency side, as electrical charges accumulate in the transducer, displacement increases in proportion. This phenomenon also causes the current input and velocity output following the same trend of a sharp rise and fall. At 2.25 and 10 MHz, both displacement and velocity outputs show slower rise times and delayed fall. At still lower frequency, V101 has four-times slower rise for the displacement and velocity outputs, resulting in the entirely different output waveforms from those of I_{in} and dV_{in}/dt. The observed varied displacement or velocity responses arise from the finite propagation speed of elastic waves and resultant electric charge generation. The elastic wave front is partially reflected at the back surface, producing opposite charges. This leads to decreasing output voltages and a negative peak in velocity, also resulting in resonance effects. In V101 and V104, the peak-to-peak duration in velocity of ~1 and 0.3 μs can be seen corresponding to the respective nominal center frequency.

Concerning the McMillan conditions, the input current and time-derivative of V_{in} are in phase with the velocity output only for the higher frequency transducers (V107 (5) and V111 (10)). V104 (2.25) is a borderline case, while V101 (0.5) shows a delayed velocity output, which

indicates a large phase lag from dissipative response. Thus, V107 and V111 satisfy the McMillan phase condition, but V101 and possibly V104 do not. It is noted here that FC500 (2.25) transducers, which will be discussed later, also satisfy the McMillan conditions because I_{in} and dV_{in}/dt are in phase with their waveforms matching better than in the case of V111.

Another behavior of transmission waveforms is shown in Fig. 11. This is for V192 (1), which has capacitive response in LCR measurement and the phase angles less than –70˚ in Z testing with HP 4800A. The observed dV_{in}/dt curve has a sharp initial spike for capacitor charging, but actual charging current shows a delay. Displacement response is further delayed, taking additional ~0.3 μs to the peak. Input current and velocity output have no correspondence. This was also seen in V189 (0.5) and V195 (2.25). V195 has actually inductive reactance as noted earlier. These large-diameter transducers have no correlation among four other curves. All three do not satisfy the 90˚ out-of-phase condition and also show phase lags, indicative of dissipative system. This is expected since these are designed with damping for broadband service. Thus, all three of them fail the McMillan conditions. REF-VL (also to be discussed) shows a similar dV_{in}/dt and I_{in} responses. The peak of dV_{in}/dt is reached at 40 ns, while I_{in} peak takes 100 ns, again showing a delay. While its velocity response was not determined, this transducer is also expected to fail the McMillan conditions.

2.4 Receiving sensitivity and comparison to transmission sensitivity

We measured voltage receiving sensitivity to displacement input, R, for many transducers and, for some, voltage receiving sensitivity to velocity input was also reported previously. In addition, two types of receiving sensitivity can be defined in terms of short-circuit current and we have the following four types:

R	voltage receiving sensitivity to displacement input
R’	voltage receiving sensitivity to velocity input.
R_c	current receiving sensitivity to displacement input
R'_c	current receiving sensitivity to velocity input.

Conversion from R to R’ can be done by $2\pi f$ division in the frequency domain (in spite of erroneous comment to the contrary in [12]). The voltage receiving and current receiving sensitivities are related by the output impedance, Z_{out}, i.e., $R = R_c Z_{out}$ and $R' = R_c' Z_{out}$.

Two transducers newly examined (V107 (5) and V111 (10)) showed relatively flat R’ response within ±5-dB to 4 MHz. Correspondingly, both showed well matched waveforms between the velocity input and voltage output in face-to-face experiments. In contrast, V101 (0.5) and V104 (2.25) that had similarly flat R’ response below the nominal center frequency exhibited no such matched waveforms.

In the following two figures, receiving sensitivity spectra are plotted, representing R (in red curve: V/nm), R’ (in blue curve: Vs/m), R_c (in red dash curve: A/nm), and R'_c (in blue dash curve: As/m). The two top (blue) curves are velocity sensitivities and two bottom (red) curves displacement sensitivities. Fig 12-a is a graph showing the four receiving sensitivity spectra of

V192 (1). The two middle curves (R and R'_c) are of similar shapes with average separation of 7.4 dB for V192 and 11.1 dB for R15 (to 2 MHz), shown in Fig. 12-b. In all other transducers, the differences were less and V101 and V111, in particular, showed nearly matching behavior (average differences of 0.6 and 0.05 dB to 2 MHz). Again, V195 (2.25) behavior was completely different from those of other transducers.

In order to examine if any agreement between the transmission and receiving sensitivity spectra exists, all eight sensitivity spectra are plotted together. Three examples are given in Fig 13. V101 (Fig. 13-a) has two pairs of spectra close together, but these are the pair of transmission or receiving sensitivities, not between transmission and receiving. Fig 13-b for V195 is an example of complete mismatch. R15 spectra shown in Fig 13-c contain one pair of t'_c and R'_c, that has two curves close by. The average difference is 3 dB to 2 MHz, but the standard deviation is 6.1 dB and this pair can hardly qualify as similarly shaped spectra.

Despite apparent mismatch, pairs of t'_c and R'_c are often used in the discussion of reciprocity. Thus, we evaluated the average of standard deviation of their spectral differences. Since pairs of t_v and R are displacement equivalent, these were also considered. Results are shown in Table 1. The results for the t_v - R pairs are as expected with the standard deviation of more than 6 dB. However, comparable data for the t'_c and R'_c pairs are in the range of 1.5 to 2.5 dB (except V195 and R15, which are non-reciprocal transducers). This modest agreement is hard to interpret at this stage because of experimental uncertainties. If this is taken as an agreement, then, the Schmerr condition is satisfied. But this group includes those proven to be non-reciprocal earlier, like V101, V192 and possibly V104. Thus, it is unlikely that the transmission sensitivity spectra and receiving sensitivity spectra are identical for all the transducers examined.

In our previous work [12], this aspect was examined from the shapes of transmitted and received waveforms. Under an impulse excitation, typically, the former is a monopolar pulse while the latter a bipolar one. Redwood [17] first discussed the origin of this behavior. He attributed the monopolar transmission to the absorption of back-propagating displacement pulse and the bipolar receiving to the pulse reflection at the back surface. In reception, while most of mechanical pulse is transmitted into the backing, electrical charge is reflected, resulting in a pulse of opposite polarity. This model was verified [12] using both damped and undamped piezoelectric transducers. This provides the physical foundation for the lack of reciprocal behavior.

2.5 Ratio of receiving sensitivity and transmission sensitivity

Of many possible pairings of spectral curves, we need to further examine the case of current-velocity transmission sensitivity and displacement- or velocity-voltage receiving sensitivity. The current-velocity transmission sensitivity is the parameter most commonly used in reciprocity calibration methods. For the receiving sensitivity, the input to a receiver has been chosen to be either displacement (or force) or velocity while the output is usually measured in open-circuit voltage. For our transducers, load resistance above 10 kΩ was adequate. These two receiving sensitivities are related by a factor of $2\pi f$ as noted earlier.

For any transducer, we can define a ratio of receiving and transmission sensitivity spectra, as it has been done since MacLean [3]. Let us define

$$J = R / t'_c \text{ and } J' = R'/t'_c, \qquad (3)$$

where J-parameter uses displacement-voltage receiving sensitivity and J'-parameter refers to its velocity input counterpart. When J' (or J) for two transducers are equal, these form a reversible pair that satisfies the reversibility condition. Next, it is arbitrarily postulated that the J' values should agree within ±0.5 dB with each other. This requirement is needed since we utilize this reversibility condition as the basis for reciprocity calibration methods with the target of achieving 1 dB accuracy. Here, this 1-dB accuracy target is equivalent to the goal adopted in ASTM 1106/ISO12713 for the primary sensor calibration [1]. The above requirement for J'-parameter is a difficult goal to achieve, but it is indeed necessary for meaningful reciprocity calibration. Practical target values of less than 0.5 dB spectral difference and standard deviation under 1 dB may be used for satisfactory matching (although these are still inadequate for reaching the 1-dB accuracy target).

From the experimentally determined values of R, R', t_v and t'_c for the nine transducers in this study, J- and J'-parameters were calculated. First, J values are plotted against frequency in Fig. 14. All curves show nearly parallel behavior and logarithmic trends in the dB-(linear) frequency plots. Three groupings are recognized, corresponding to 38-mm, 25-mm and 13-mm transducer diameters. The top group is ~7 dB higher than the middle group, while the bottom group is ~12 dB lower than the middle. It was previously shown that receiving sensitivity must be corrected for the sensing area differences to compare their responses to each other. With the size correction of -7.05 dB and +12.05 dB applied and using the J'-parameter, we obtain Fig. 15. The main feature is that these curves do not coincide within the desired range of ±0.5 dB. On the other hand, we observe relatively flat curves that are within a several-dB-wide band. The average of all data points to 2 MHz excluding obvious outliers (<100 kHz for V195 (2.25), >1 MHz for R15 (0.15) and V101 (0.5)) was 75.9 dB. If the accuracy of ±5 dB is tolerated, this value can be used for J'. Obviously, such a large error is not acceptable. Thus, it is difficult to recognize the existence of reversibility conditions by any combination of these transducers. That is, these pairings do not satisfy the MacLean condition. Obviously, these are J' of different models of UT/AE transducers and we need to examine the case for identical transducers.

Let us next consider two sets of identical transducers. One set is of three PAC R15 resonant sensors. The other set consists of three AET FC500 sensors, which were nominally 2.25-MHz damped UT transducers. In these tests, we used a different current probe, constructed using a current transformer with small ferrite beads, pulse-calibrated with known capacitors and resistors. (See Appendix for its construction details.) Z measurements thus obtained agreed to static impedance values from a vector impedance meter (HP 4800A) to better than 0.5 dB. J' vs. frequency results for the two sets are plotted in Fig. 16. The bottom group is the curves for R15. Clearly, large scatters of 5 to 10 dB persist at all frequencies with the standard deviation of 2.29 dB to 1 MHz. This apparently arises from different transmission and receiving sensitivities at

various resonance points. Clearly, these J' data for R15 sensors exhibit no reversibility. (This data set received no size correction of 12 dB addition since FC500 data would be obscured.)

In a sharp contrast to the R15 behavior, the three top curves for FC500 coincide very well once the frequency exceeds 100 kHz. Above this frequency, the three traces overlap each other even when small peaks and valleys are present. The standard deviation among the three spectra averages to 0.39 dB to 2 MHz and it is further reduced to 0.29 dB excluding the range below 100 kHz. This set can be deemed to satisfy the reversibility condition when any two of the three are combined. By using identical models having relatively smooth spectra, it is possible to achieve the reversibility condition we set forth in this section.

2.6 Quantitative reversibility tests

The inequality of transmission and receiving sensitivities has now been demonstrated, but we observe that the presence of the reversibility condition depends on the selection of a particular transducer pair. In the previous study, we evaluated the reversibility in terms of voltage-displacement-based transmission-receiving sensitivity spectra. The reversibility was often absent, especially after applying the receiving-sensitivity correction for the sensing area. Average difference of combined spectra typically ranged from 5 to 20 dB. In the present study, current-based transmission spectra are also used together with velocity-voltage receiving sensitivity. In this section, we evaluate quantitatively the average spectral differences and the standard deviation for various transducer pairs. Numerical results can show how close each pair is with respect to reaching the reversibility condition.

One approach is to use J'-parameters examined in the preceding section (cf. Fig. 15). Dividing (subtracting in dB scale) J' for transducer t1 with J' for transducer t2, we have the ratio of $R'_{t1}\, t'_c{}^{(t2)}$ and $R'_{t2}\, t'_c{}^{(t1)}$. That is,

$$J'_1 / J'_2 = R'_{t1}\, t'_c{}^{(t2)} / R'_{t2}\, t'_c{}^{(t1)}. \qquad (4)$$

When this ratio is unity (a J' difference of 0 ± 0.5 dB), the reversibility is observed. Results for J'-ratio are shown in Table 2 for ten pairings in the frequency ranges of 22 kHz to 1 MHz or 2 MHz. Average values of the ratio and the standard deviation (in dB) are given in the top four rows. For the case of V195 (2.25), the range below 100 kHz was excluded as deviation was large. Of the twenty cases, ten results give the average value within ±1 dB and the rest ranges up to 5 dB. Even when the average is low, the standard deviation always exceeds 0.9 dB, reaching 3 dB. This value goes up to 9 dB in two high average cases. When a resonant R15 (0.15) sensor is a part of pairing, both the average and standard deviation are higher than those for UT transducer pairs. The fifth row gives the average difference of input current spectra, ranging from 6 to 21 dB, offering an estimate of the current effect on the ratio of J' above. The next two rows give comparable data for the voltage-based transmission-receiving spectra pairing and clearly show much larger difference values. The values of the standard deviation are also higher, indicating the current-based transmission sensitivity improves reversibility for the combinations examined here. The next row gives the ratio of input voltage spectra, which

shows less variability than the current ratio. The last row gives size correction applied in computing the ratios of J' and those of R' t_v.

Regardless of the choice of driving input variable, the observed levels of standard deviation are unacceptable as the basis of any calibration since the maximum deviation typically goes up to four-times that of standard deviation. Thus, we find no reversibility among the combinations examined here. These pairs fail to satisfy the MacLean's reciprocity condition.

The second approach for the reversibility validation is to compare the measured voltage sensitivities from a transducer pair in both directions, t1 to t2 and t2 to t1. By dividing the transmission side with corresponding input current spectrum and adding the receiving sensitivity, the comparison becomes identical to the first approach, but using experimental sensitivities data. That is, the combined data was reconstituted from separately determined values of t'_c, I_{in}, and R'. Results are given in Table 3, part a). Size correction was applied when the receiver size is larger than the transmitter size. Without this correction, observed levels of spectral matching are absent when the receiver size is larger than the transmitter. The values of the correction are listed in the bottom row. The average spectral differences are listed in the 2nd row, ranging from 0.03 dB to 1.97 dB. Four examples are graphically plotted in Fig. 17. These pairs of curves have reasonably good match. This level of agreement is typically deemed to exhibit the reversibility in the literature. In terms of the tabulated data, the average spectral differences, ΔPS, are below ±1 dB in seven out of 8 cases. However, the level of the standard deviation was not reduced at all, showing 1 to 3 dB as before. This last point has been ignored in all previous qualitative estimation of reversibility. However, this is crucial in achieving the desired accuracy in calibration. Thus, only one case of V189 (0.5)-V192 (1) pair satisfies the reversibility criteria (<0.5-dB average and <1-dB standard deviation).

The third comparison method is to utilize the voltage output from face-to-face tests. Normalization with the input current spectrum can also be applied, while input voltage normalization can be omitted as the voltage spectra varies little. The results of spectral differences, ΔPS, are shown in Table 3-b). For voltage input data on the first row and the current input data on the 2nd row, corresponding to transducer pair listed at the top row in part a). ΔPS for the voltage input varies from 0.18 to 18 dB, while those of the current input vary from 0.08 to 0.68 dB. The discrepancy between the voltage and current input data comes from the inclusion of the input impedance, Z_{in}, of the transducers. When the difference of Z_{in} for the particular pair is included, the discrepancy is reduced to at most 3.5 dB. When Z-correction is added, one pair satisfies the reversibility condition, while one more nearly clear the criteria. The current input data shows smaller ΔPS generally, but the cases satisfying the reversibility condition are comparable. Voltage input data without the Z correction is the worst regardless.

Six additional cases of the face-to-face tests are examined (Table 3-c). These all have the same transducer sizes. As shown in part c), results are slightly improved, but the use of V195 (2.25) made it impossible to achieve reversibility. This is due to its large differences in the transmission and receiving sensitivities below 200 kHz. When this part is excluded, ΔPS data become comparable to other pairs.

From the above findings, the level of spectral agreement is generally insufficient to confirm the reversibility condition when transducers of different types are combined except in a small fraction of cases with similar transducer design.

When transducers of the same type are combined to form transmitter-receiver pairs, one expects improved reversibility. Three sets of identical transducers were examined for their reversibility. These are PAC R15 (0.15), PAC R6a (0.06) and AET FC500 (2.25). In the previous report, the voltage-based transmission-receiving spectra for the pairing of FC500 exhibited good reversibility in graphical presentation, but we did not compute the statistics of spectral similarity. Here, we include current-based spectra pairings as well.

Figure 18 shows the spectral results of a pair of FC500 (#280 and #281) indicative of an excellent reversible behavior. This is also reflected in the numerical results. Over a wide frequency range from 20 kHz to 4.5 MHz, the average spectral difference was 0.01 dB and the standard deviation was 0.37 dB. When the spectra are corrected for the input current spectra, both the average difference and standard deviation increased slightly. In two other pairings, numerical results are similar as shown in Table 4-a. Effects of current correction were mixed, reflecting the ratio of input current spectra differing 0.16 to 0.39 dB. In contrast, the voltage ratios had spectral differences below 0.01 dB. These transducers represent a damped, broadband design aimed at 2.25 MHz applications and no resonance peak is evident. These satisfy the reversibility criteria set earlier. That is, these FC500 are fully reversible.

Figure 19 exhibits the comparison of R15 spectra. These are resonant sensors of high sensitivity, and the spectra contain many peaks and valleys. Top two curves compare voltage-based displacement sensitivities ($T_i + R_j$), while the lower curves are corrected for the input current spectra ($T_i - I_{in,I} + R_j$), both sets exhibiting good reversibility. When we limit the upper frequency at 500 kHz, the average spectral differences are within the 0.5 dB limit. The tabular results (Table 4-b) also indicate that the 1-dB standard deviation limit is nearly met; it is slightly exceeded in three of six cases. Current correction typically worsens the values. These R15 sensors can be treated as reversible up to 600 kHz. Above this range, there are non-matched zones at 650 to 850 kHz and statistics become poor, but this is out of intended application frequency range.

Figure 20 shows the results of another set of resonant R6a sensors of high sensitivity for low frequency applications. As in Fig. 19, the voltage- and current-based sensitivity curves are shown at top and bottom, respectively. The average spectral difference limit is almost met when we use the voltage-based sensitivity over 22 to 500 kHz range. However, current-based sensitivity makes the spectral difference over the limit. In this sensor set, the standard deviation remains high; always exceeding 2 dB (Table 4-c). The spectral curves mismatch most at spectral valleys: when we exclude the values below 80 dB, the standard deviation is almost reduced to the 1-dB limit. In this figure, the smooth-rising dashed curves are for the input current spectra. That is, these I_{in} curves show no fluctuating behavior of the sensitivity curves, implying the resonance behavior is linked to mechanical resonance coupled to the sensing

element rather than the input electrical impedance. This may contribute especially to poor spectral matching at anti-resonance frequencies found here. These R6a sensors cannot be regarded as reversible.

From the evaluation of matching and non-matching transducer pairs, the reversibility behavior can be expected only in well-damped broadband transducer pairs of similar internal construction. For identical resonant sensor pairs, reversibility may or may not exist as seen in our two such sets. The non-matching transducer pairs almost always failed to show the reversibility.

In the above evaluation of reversibility, the current-velocity transmission (t'_c) and velocity-voltage receiving (R') sensitivities were paired to show spectral similarity, although exact spectral matching was not observed. Symmetry suggests that voltage-velocity transmission (t'_v) and velocity-current receiving (R'_c) sensitivities can be paired to produce comparable spectral similarity. This is actually a consequence of the matching (except at resonances) of input and output impedance values ($Z_{in} = Z_{out}$), since we have the following relationship:

$$t'_c R' = t'_v R' Z_{in} = t'_c R'_c Z_{out} = t'_v R'_c. \quad (5)$$

Since the comparison of Z_{in} and Z_{out} was given in Fig. 7, additional graphs are skipped here.

3. Discussion

3.1 Transducer behavior

From the preceding study [12] and present work, we have gained the following understanding in regard to the behavior of UT/AE transducers.

1. The transmission behavior of higher frequency transducers (V111 (10), V107 (5) and FC500 (2.25)) exhibited good agreement between input current and output velocity, satisfying the McMillan condition. Most others failed this criterion since a response time delay developed, corresponding to a phase lag. In some transducers, complete mismatches are found among various waveforms including delayed velocity responses. V195 (2.25) totally failed the McMillan condition due to its resistive/inductive behavior.
2. The transmission sensitivity spectra and receiving sensitivity spectra are different and distinct for all the transducers examined. Although t'_c and R' spectra have similar shapes, the degree of matching is found to be inadequate. The Schmerr condition is not met. Transducers generally exhibit differing ratios of receiving and transmission sensitivities unless they are of identical design and construction, thus failing the MacLean condition. This exception was observed when FC500 transducers were examined (cf. Fig. 16). The ratios do fall into a relatively narrow data band (Fig. 15).
3. The reversibility behavior can be expected only in well-damped broadband transducer pairs of similar physical construction. For identical resonant sensor pairs, reversibility may or may not exist. The non-matching transducer pairs almost always failed to show the reversibility.

4. The input and output electrical impedance of these transducers agree with each other except where resonant behavior is found.

From these findings, it is concluded that a pair of an arbitrary transducer with any of the transducers tested above is unlikely to exhibit the reciprocal behavior unless it is of identical model that shows the capacitive response without resonances.

3.2 Calibration methods

Displacement sensitivities can be determined using the direct or indirect methods based on laser interferometric calibration as reported in the previous study [12]. The indirect method relied on forward-reverse measurements, but the reversibility condition was not used. The tri-transducer method (TTM) was introduced and was used to obtain consistent displacement-based calibration. Here, TTM is found to be the displacement-equivalent of Hill-Adams equation, which requires input current measurement. In this work, it has been shown that these four methods provide mutually consistent calibration for all the transducers without the need of establishing the condition of reversibility or reciprocity.

Experimentally, it is also shown that impedance measurement can be used in lieu of input current, or vice versa, as expected by their definition. Impedance analyzers are more common instrument in laboratory than current probes. These are needed when one requires current-based transmission sensitivity, but not for receiving sensitivity determination.

3.3 Reexamination of reciprocity calibration methods

The classical reciprocity calibration methods assumed the reversibility of any transmitter-receiver combination output, or $E_{ij}/I_{ij} = E_{ji}/I_{ji}$, for a pair of transducers i and j (or ti and tj) with input current of I_{ij} or I_{ji}. Now, we have observed that this condition exists only for limited cases of identical transducers having smooth sensitivity spectra. In the absence of general reversibility, it is necessary to reexamine the validity of prevailing reciprocity calibration methodology.

One common approach is to use the sequential (1-2-3) transducer combination and to construct the formulation in terms of the current-velocity transmission (t'_c) and velocity-voltage receiving (R') sensitivities of three transducers. For example, Hatano and coworkers [13, 14] and Japanese NDIS2109 standard [18] derived from their work utilize this sequential transducer combination. This was also used by Herve et al. [19]. The ratio of the two sensitivities leads to J' parameter defined earlier in eqn (3) as $J' = R'/t'_c$. The standard reciprocity parameter is a combination of J' and the transmission transfer function, X, for the medium, through which transducers i and j are acoustically coupled. In the face-to-face method, X = 1. Then, $E_{ij}/I_i = t'^{(i)}_c X R'_j$, assuming X to be a geometrical constant (although it is known that X depends on the transducer sizes, propagation distance and frequency). That is, we have for the 1-2-3 sequence

$$E_{12}/I_1 = t'^{(1)}_c X R'_2,\ E_{23}/I_2 = t'^{(2)}_c X R'_3, \text{ and } E_{31}/I_3 = t'^{(3)}_c X R'_1. \quad (6)$$

Combining these three equations in (6), one gets

$$(E_{12}\,E_{31}\,I_2)/(E_{23}\,I_1\,I_3) = (t'^{(1)}_c\,R'_2\,t'^{(3)}_c\,R'_1\,X)/(t'^{(2)}_c\,R'_3) \qquad (7)$$

Using $J'_i = R'_i/t'^{(i)}_c$, we can eliminate three t'_c terms in (7) and obtain

$$R'_1 = [(J'_1\,J'_3/J'_2)\,(E_{31}\,E_{12}\,I_{23}/E_{23}\,I_{31}\,I_{12}\,X)]^{0.5}. \qquad (8a)$$

Similarly, we can also get

$$R'_2 = [(J'_2\,J'_1/J'_3)\,(E_{12}\,E_{23}\,I_{31}/E_{31}\,I_{12}\,I_{23}\,X)]^{0.5}, \qquad (8b)$$
$$R'_3 = [(J'_3\,J'_2/J'_1)\,(E_{23}\,E_{31}\,I_{12}/E_{12}\,I_{23}\,I_{31}\,X)]^{0.5}. \qquad (8c)$$

This derivation of eqn (8) did not use the condition of reversibility or reciprocity. However, the right side of (8a)-(8c) each contains unknown value of J'_i. That is, the unknown receiving sensitivity is expressed in terms of its own J', which is also unknown.

This is where the condition of reversibility or reciprocity is introduced. With MacLean's reciprocity condition of equal reciprocity parameters, $J'_1 = J'_2 = J'_3 = J'$, the first term in (8) becomes simply J'. With Schmerr's reciprocity condition of $M = S^{\circ}$, J' = 1, leaving only the X parameter in eqn (8). When X is unity in the face-to-face methods, we have $R' = t'_c$ and both are given by eqn (8).

Without using the reciprocity condition, but with the reversibility of the pair 1-2, (7) can be rewritten by reversing the first 1-2 pair to generate E_{21}/I_2. Then, we have

$$(E_{21}\,E_{31}\,I_2)/(E_{23}\,I_2\,I_3) = (t'^{(2)}_c\,R'_1\,t'^{(3)}_c\,R'_1\,X)/(t'^{(2)}_c\,R'_3)$$
$$= (E_{21}\,E_{31})/(E_{23}\,I_3) = ((R'_1)^2\,t'^{(3)}_c\,X)/R'_3 = ((R'_1)^2\,X)/J'_3, \qquad (7a)$$

where two t'_c terms cancel out. It can be rewritten for R'_1 as

$$R'_1 = (J'_3\,E_{21}\,E_{31}/E_{23}\,I_3\,X)^{0.5}. \qquad (2a)$$

This equation is identical to Hill-Adams equation (2) with different sensitivity notation. We do require knowing J'_3 in order to determine R_1. Actually, we can use the reversed pair 2-1 without relying on the reversibility of the pair 1-2. Then, this becomes 2-2-3 (a variation of the 1-1-3) sequence and is no longer the 1-2-3 sequence.

The usual reciprocity calibration procedure needs to assume $J'_1 = J'_2 = J'_3 = J'$ and shrinks the first term of eqn (8) into J'. Since J' for each transducer is known to be different, as shown earlier, J'_1 of the transducer-under-test cannot be canceled out by those of other transducers. When t2 and t3 constitute a reversible transducer pair with identical J', J'_2 and J'_3 are factored out, leaving only the unknown J'_1 in the equation for R'_1. Either way, we must know J'-

parameter for the transducer-under-test. This is untenable and the sequential combination cannot be utilized in the reciprocity calibration methods.

Another approach of reciprocity calibration methods uses the 1-1-3 transmitter-receiver combinations of (t1>t2, t1>t3 and t3>t2). This set-up requires no reversibility condition and current measurement is not needed for the transducer-under-test. It does limit to obtaining R'_2 and $t'_c{}^{(1)}$ (or R'_1 and $t'_c{}^{(2)}$ in 2-2-3 sequence). In terms of J'_3, we obtain Hill-Adams equation for the velocity-voltage receiving sensitivity for transducer 2 as

$$R'_2 = [(J'_3 E_{12} E_{32} / E_{13} I_3 X)]^{0.5}, \qquad (2c)$$

where I_{12} and I_{13} are factored out. This is justified as the input current is unaffected by acoustic loading of the transducer face when it is driven by a pulser that relies on capacitive discharge. During the derivation of this Hill-Adams equation, we only rely on experimentally measured values without any change in the signal direction. However, it is essential to have J'_3 determined independently of the 1-1-3 combinatory measurements. Additionally, we have

$$J'_3 / I_3 = R'_3/(t'_c{}^{(3)} I_3) = R'_3/(t'_v{}^{(3)} V_{in}{}^{(3)}) = R'_3/T'_3 = R_3/[(2\pi f)^2 T_3]. \qquad (9)$$

where $V_{in}{}^{(3)}$ is the driving voltage and T_3 is the displacement output of transducer 3 driven by $V_{in}{}^{(3)}$. Thus, when T_3 is available from laser interferometry for a pulser-transducer combination, no driving current measurement is required. We then get

$$R'_2 = [(E_{12} E_{32} / E_{13} X)(R'_3/T'_3)]^{0.5} = [(E_{12} E_{32} / E_{13} X)(R_3/(2\pi f)^2 T_3)]^{0.5} \qquad (10)$$

When we multiply 2πf on both sides, this is identical to the expression introduced previously as the tri-transducer method (though X = 1 was used for the face-to-face set-up). That is,

$$R_2 = [(E_{12} E_{32} / E_{13} X)(R_3/T_3)]^{0.5} \qquad (11)$$

Thus, this tri-transducer method (TTM) is not a new method and should be considered as the displacement expression of Hill-Adams equation. This also proves the validity of interpreting E_{ij} as the product of T_i and R_j as we have used in [12]. Following the derivation of eqn (1) in terms of T and R without using the input current, we can deduce the product of R and T. Also avoiding the reversibility condition, we can define the R-T product for i-th transducer (for I, j, k of 1 to 3) as

$$(R \cdot T)_i = E_{ij} E_{ki} / E_{kj}, \qquad (12)$$

As before, we take X = 1 for the face-to-face set-ups. Since this derivation does not utilize the conditions of reversibility or reciprocity, no separate proof is required of its use. It can thus be used to verify other calibration results. (We still retain “reciprocity” term for continuity’s sake, but only Hill-Adams method can be utilized.)

3.4 Validation of Hill-Adams method

In the previous work [12], we showed that the TTM gives displacement sensitivities in agreement with the direct or indirect methods based on laser interferometric calibration. Although this may be superfluous, we present a few examples of matching calibration results for velocity sensitivity between Hill-Adams method and laser-based direct method.

Figure 21 shows results of Hill-Adams calibration of PAC F30 (0.3) sensor using V192 (1) as a transmitter and V103 (1) as a reference. This figure plots E_{ij} for V192 to F30 (red dash), V192 to V103 (purple dash), V103 to F30 (blue dash), J'_{V103} (green), I_{V103} (brown dash), R' for PAC F30 sensor (red) by Hill-Adams method and R' for F30 by the direct method (blue curve). These two R' spectra differ by 0.65 dB on average over 50 to 600 kHz with the standard deviation of 0.79 dB. A good agreement is obtained.

Figure 22 compares R' spectra from Hill-Adams method (solid curves) and direct method (dashed curves) for PAC R15 (0.15) sensor (blue curves) and Fuji Ceramics REF-VL (0.3 – green curves). The average differences and standard deviation between the two methods are summarized below.

F30 (AA20)	0.65 dB	0.79 dB	(50-600 kHz)
R15 (BS90)	0.24	1.17	(50-600 kHz)
REF-VL (#692)	0.75	0.52	(50-1000 kHz)

The last two cases also give good agreement between the two methods. Agreement can be improved further using a reference transducer with smoother J'-parameter than V103 used here. This V103 does have oscillating J' curve (green) at lower frequencies as shown in Fig. 21. Yet, satisfactory results are obtained using Hill-Adams method. We have compared a dozen other cases, and all provided similarly satisfactory outcome.

In the above computation of Hill-Adams method, we used the ratio of R' and T' obtained from the direct method. While we did measure input current using a modern current probe that utilizes Hall-effect sensing or a current transformer with ferrite beads, this was unnecessary after all. Still, t'_c of a transducer is obtained from the sensor's displacement output (T) using the current measurement, the displacement spectrum is the basic characteristic of a transducer along with its electrical impedance (Z). Impedance measuring instrument is more commonly available in laboratory and this can be used in lieu of current probes.

We have now demonstrated that Hill-Adams method can provide satisfactory calibration of receiving sensitivity of UT/AE transducers either in velocity-voltage or displacement-voltage mode. This method does need a reference transducer with known spectral ratio of R' and T' (or R and T) that have previously been determined using the direct method based on laser interferometry or using equivalent methods involving hydrophone calibration facility. However, this method does not need to confirm the reversibility or to measure the driving input current.

3.5 Existing standards

A national society level standard exists for AE sensor calibration based on a reciprocity technique. This standard, NDIS2109 [18], was written based on papers by Hatano and coworkers [13, 14] and issued by Japanese Society for Non-Destructive Inspection. Currently, it is being considered to be an ISO standard (ISO-TR13115). However, this document contains numerous issues in need of change, removal or clarification even when we restrict our discussion for the longitudinal wave case only.

1) It specifies the use of the sequential combination set-up, which has been shown here as unworkable. This difficulty arises because of required inclusion of an unknown parameter, that is, J' of the transducer being tested, in the equation for sensitivity calculation. The standard invokes the reciprocity condition, equating the reciprocity parameters of all transducers without validation. Actually, this is impossible to achieve because one of the three is being calibrated. Obviously, we do not possess J' parameter for this test article.

2) This standard utilizes the reciprocity parameter (H = S/M) that only depends on the wave propagation through a solid medium. It has been demonstrated by Hill and Adams theoretically and proven here experimentally that S˚ and M are distinct for each transducer, cannot be treated as equal and their ratio is independent of geometrical conditions. The transducer proper S˚/M ratio (we defined it as 1/J') must be a part of the sensitivity equation.

3) This standard declares that any transducer is reciprocal when it can transmit or receive a wave and this reciprocity declaration has no other conditions. Even the reversibility condition is not included.

4) Although not stated clearly, it appears that NDIS2109 treats reciprocity to mean a single reciprocity parameter H for all three transducers. Since H for the transducer-under-test is unknown, this makes no scientific sense and requires validation.

Another serious drawback of this standard is the lack of credible validation. The main justification for the method is comparative study conducted in 1980s with the NIST group that pioneered the seismic impulse calibration (ASTM 1106 [1]). However, the NIST group discontinued their effort on the longitudinal wave calibration and no follow-up study has been made. We can find no validation of reciprocity parameters used, or of wave propagation through the transfer block for various transducer combination. Thus, this standard is need of serious reexamination by the standards committees that certified it originally and developed it into an international document.

3.6 Limits of calibration methods

We have observed that a set of three FC500 (2.25) transducers have reversible behavior. Using measured values of E_{ij}/I_i, let us explore the limits of the calibration procedures in our study. The sensitivities, R and T, of these transducers have been obtained by the direct and indirect methods, as shown in Fig. 23. For these tests, V104 (2.25), V107 (5), V192 (1) and V195 (2.25) transducers with known T and R values were utilized. The top three curves are for T, while the bottom three curves R. The middle three solid curves represent the geometric mean, $(R\,T)^{0.5}$. These are from the laser-based methods.

For this set, good reversibility is observed among FC500 transducers and we have determined E_{ij} values for all combinations of three FC500 (cf. Fig. 18). These E_{ij} values can be utilized to calculate $(R\ T)^{0.5}$ for these FC500 using eqn (12). The dashed curves in the middle group of Fig. 23 are from eqn (12) based on the Hill-Adams equation and measured E_{ij} values.

The same data are given in an enlarged scale in Fig. 24. Again, the solid curves are for the direct/indirect results while dashed ones represent the values from the method based on the Hill-Adams equation (eqn (12)). The corresponding curves are within 1.5 dB of each other up to 2 MHz. Here the two sets of curves match modestly with the average difference of 0.40, 0.60 and 0.92 dB. In the range of 2 to 3.5 MHz, the differences increase and reach 5 dB. An apparent peak is present centering at 2.7 MHz. Also plotted in this figure are three curves of $(R\ T)^{0.5}$ from the TTM that utilized V195 or V192 and V104 as additional transducers. These are shown as dotted curves and overlap the curves based on the Hill-Adams equation closely up to 2 MHz. The average differences of 0.02, 0.24 and 0.68 dB to 2 MHz were observed with the standard deviation of less than 0.5 dB. The curves start to separate above 2 MHz, but the difference remains less than 2 dB. The average differences were 0.65, 0.70 and 0.82 dB to 4 MHz, which are still moderately good matches.

The observed discrepancies in $(R\ T)^{0.5}$ above 2 MHz point to less firm foundation of direct calibration method at higher frequencies. The reference transducers that can provide smooth transmission spectra are limited to V104 and V195 with V107 used as an auxiliary unit. In the particular range of 2 to 3.5 MHz, these three usually produce two results matching and one slightly off. Presently, these are averaged, but we need additional references to increase the reliability at higher frequency. Currently, direct method with laser interferometry and indirect method produce matching while the TTM and Hill-Adams method provide another matching result. We continue to explore approaches that make them into unique spectral output.

Thus, direct method with multiple well-behaved reference transducers gives the most reliable outcome, followed by indirect, TTM and Hill-Adams methods for frequency up to 2 MHz. The accuracy is estimated to be approximately 1 dB. The accuracy in higher frequency range is lower by as much as 5 dB and additional efforts are required for improvement. Here, we need a better laser interferometer with lower noise above 5 MHz, a better pulser with a shorter pulse rise time and more reference transducers. While the first approach is a costly proposition, a faster pulser may be achieved by inserting an FET driver. However, high-current FETs have a switching time of about 40 ns even today and other methods must be explored. Getting more reference transducers is a feasible option. Current sensing always adds additional source of uncertainty and is not recommended unless current-based transmission sensitivity is specifically required.

4. Conclusions

1. From systematic evaluation of over twenty transducers, we have determined their transmission and receiving sensitivity spectra. In each of the transducers, these spectra are different and distinct even when identical units are compared. Transducers generally exhibit

differing ratios of receiving and transmission sensitivities, J', except when they are of identical design and construction. In this exceptional case, three broadband transducers (FC500) exhibited mutually reciprocal and reversible behavior. In all other combinations, some pairs were reversible, but not reciprocal.

2. Most of the transducers by themselves or in combination failed to satisfy the conditions of reciprocity and reversibility. This is especially true for transducers of damped piezoelectric design and for those of enhanced sensitivity with resonance effects. The methods for calibrating these need to avoid requiring these restrictive conditions.
3. Four methods of transducer calibration, direct, indirect, TTM and Hill-Adams methods, provide mutually consistent results for the transmission and receiving sensitivity. These require no reciprocity or reversibility conditions. Input current sensing is only required in obtaining the current-based transmission sensitivity, but it increases data scatter and is not usually needed. Besides, electrical impedance measurement can be substituted for the current sensing.
4. Reciprocity calibration methods are critically examined. One variation, known as Hill-Adams method, uses no reversibility or reciprocity condition in the derivation. This method does require independent determination of the J' parameter for a reference transducer. Another variation that relies on the sequential combinations results in the sensitivity equations containing unknown variables on both sides of the equations. This serious flaw can only be eliminated by introducing the MacLean reciprocity of equal reciprocity parameters for all three transducers. This generally does not exist as shown in this study and also requires the sensitivities of the transducer-under-test. Thus, this commonly used reciprocity calibration method cannot function. This implies that standards, such as NDIS2109/ISO-TR13115, have no foundation as it is based on the flawed theory and procedures.

Acknowledgment

The author is grateful for Dr. Hideo Cho, Aoyama Gakuin Univ., who conducted laser interferometry, and Dr. H. Inaba and Mr. I. Yamamoto, Fuji Ceramics, for input current measurement for this study. Discussions with Drs. H. Cho, H. Hatano, H. Inaba, and Y. Mizutani and Herr. H. Vallen were also useful.

References

1. ISO 12713: 1998(E) *Non-destructive testing - Acoustic emission inspection - Primary calibration of transducers*; ASTM E1106-12 *Standard method for primary calibration of acoustic emission sensors*, ASTM International, West Conshohocken, PA, USA, 12 p, (2016).
2. http://www.npl.co.uk/ultrasound-and-underwater-acoustics/underwater-acoustics/products-and-services/calibration-of-hydrophones-and-projectors;
Last updated on Mar. 25, 2010. Retrieved February 9, 2017.
3. W.R. MacLean, J. Acoust. Soc. Amer., **12**: 140-146 (1940).
4. L.L. Foldy and H. Primakoff, J. Acoust. Soc. Amer., **17**: 109-120 (1945).
5. R.J. Bobber, J. Acoust. Soc. Amer., **39:** 680 (1966).

6**.** L.E. Kinsler, A.R. Frey, A.B. Coppens and J.V. Sanders, *Fundamentals of Acoustics*, 3rd ed., Wiley, New York (1982).
7. B.A. Auld *Acoustic Fields and Waves in Solids*, 2nd ed., Vols. 1, 2, Krieger Publishing Co., Malabar, FL (1990).
8. C.J. Dang, L.W. Schmerr and A. Sedov, Res. Nondest. Eval., **14**: 141, 177, 203 (2002).
9. L.W. Schmerr and S.-J. Song, *Ultrasonic Nondestructive Evaluation Systems, Models and Measurements*, Springer, New York (2007).
10. R. Hill and N.L. Adams, Acustica, **43**: 305-312 (1979).
11. E.M. McMillan, J. Acoust. Soc. Amer., **18**, 344 (1947).
12. K. Ono, Materials, **9**, 508 (2016); doi:10.3390/ma9070508
13. H. Hatano and T. Watanabe, J. Acoust. Soc. Amer., **101**, 1450 (1997).
14. H. Hatano, T. Chaya, S. Watanabe, K. Jinbo, IEEE Transactions UFFC, **5**(45), 1221 (1998).
15. L. Goujon and J.C. Baboux, Meas. Sci. Technol., **14**, 903–908 (2003).
16. J. Keprt and P. Benes, P.; J. Acoust. Emiss. **26**: 60 (2008).
17. M. Redwood, J. Acoust. Soc. Amer., **33**, 327 (1966).
18. NDIS 2109-91, *Method for absolute calibration of acoustic emission transducers by reciprocity technique*, The Japanese Society for Non-Destructive Inspection, Tokyo, (1991). This is also ISO-TR13115 (2011).
19. C. Herve, S. Maillard, F. Zhang, L. Jaubert, J. Catty, and M. Cherfaoui, *Proc. The 28th European Conf. on Acoustic Emission Testing*, Cracow Univ. Tech., Krakow, Poland. pp. 1-11 (2008).

Figure Captions

Fig. 1-a Displacement output of transducers, V107 and V111.
Fig. 1-b Waveforms of pulse input (V_{in} in V) with transducer connected.

Fig. 2 Displacement output spectra for five transducers (V104, V107, V111, V192 and V195) in reference to 0 dB at 1 nm.

Fig. 3 Waveforms of pulse input (V_{in}/100 in V), current input (I_{in} in A), dV_{in}/dt (peak matched to I_{in}) for R15 transducer.

Fig. 4 Input current spectra for V101, V103 and V104 transducers in reference to 0 dB at 1 A.

Fig. 5 Input electrical impedance for nine transducers in reference to 0 dB at 1 ohm. From top, R15 (green – 0.15), V103 (red - 1), V101 (blue – 0.5), V111 (purple dash - 10), V107 (green dash - 5), V192 (dark red - 1), V189 (purple - 0.5), V104 (purple dash-dot – 2.25), and V195 (blue dash – 2.25).

Fig. 6 Input electrical impedance in dB for three transducers, R15 (0.15), V103 (1) and V101 (0.5). Static Z in solid curves and dynamic Z in dashed curves.

Fig. 7 Input and output electrical impedance in dB for three transducers, R15, V104 (2.25) and V195 (2.25). Output Z in solid curves and input Z in dashed curves.

Fig. 8 Four types of transmission sensitivities (see text for definitions) for V107 (5) together with pulse voltage spectrum (V_{in}), input current spectrum (I_{in}) and displacement spectrum (T).

Fig. 9 Four types of transmission sensitivities (see text for definitions) for R15 (0.15) together with pulse voltage spectrum (V_{in}), input current spectrum (I_{in}) and displacement spectrum (T).

Fig. 10-a Waveforms of displacement and velocity output of V101 (0.5) transducer with input pulse (V_{in}/100 in V), input current (A) and dV_{in}/dt. Displacement is divided by 5 and in nm. The velocity and dV_{in}/dt are scaled to be comparable to the peaks of other waveforms.

Fig. 10-b Waveforms of displacement and velocity output of V104 (2.25) transducer with input pulse (V_{in}/100 in V), twice input current (in A) and dV_{in}/dt. Displacement is in nm. The velocity and dV_{in}/dt are scaled to be comparable to the peaks of other waveforms.

Fig. 10-c Waveforms of displacement and velocity output of V111 (10) transducer with input pulse (V_{in}/100 in V), I_{in} (in A) and dV_{in}/dt. Displacement in nm is divided by 3. The velocity and dV_{in}/dt are scaled to be comparable to the peaks of other waveforms.

Fig. 11 Waveforms of displacement and velocity output of V192 (1) transducer with input pulse (V_{in}/100 in V), I_{in} (in A) and dV_{in}/dt. Displacement is in nm. The velocity and dV_{in}/dt are scaled to be comparable to the peaks of other waveforms.

Fig. 12-a Receiving sensitivities of V192 (1) transducer. See text for definitions of symbols.
Fig. 12-b Receiving sensitivities of R15 (0.15) transducer. See text for definitions of symbols.

Fig. 13-a Four types of transmission sensitivities and four types of receiving sensitivities of V101 (1) transducer.
Fig. 13-b Four types of transmission sensitivities and four types of receiving sensitivities of V195 (2.25) transducer.
Fig. 13-c Four types of transmission sensitivities and four types of receiving sensitivities of R15 (0.15) transducer.

Fig. 14 J ratios of R/t'_c in dB for nine transducers. From top: V195 (purple – 2.25), V189 (blue dash - 0.5), V192 (red dash - 1), V101 (green - 0.5), V104 (purple dash – 2.25), V107 (green dash - 5), V111 (purple dash - 10), V103 (blue - 1), R15 (red – 0.15).

Fig. 15 J' ratios of R'/t'_c in dB for nine transducers. Same color code used as in Fig. 14.

Fig. 16 J' ratios of R'/t'_c in dB for three FC500 (2.25) and three R15 (0.15) transducers. Additions of 5 dB for FC500 and 12 dB for R15 are needed to make J' values equivalent to nominal 25 mm diameter used in Fig. 14.

Fig. 17 Face-to-face test results for reversibility evaluation. Solid curves are for the combination of V103 (1) to R15 (0.15) (red), V103 (1) to V192 (1) (green), V192 (1) to R15 (0.15) (brown) and V101 (0.5) to V189 (0.5) (blue). Dashed curves are for the opposite signal direction.

Fig. 18 Face-to-face test results for reversibility evaluation for FC500 (2.25) pair. Blue curve for #280 to #281 and red opposite.

Fig. 19 Face-to-face test results for reversibility evaluation for R15 (0.15) pair. Blue curve for #67 to #90 and red opposite. Solid curves are voltage-based reversibility tests and dashed curves with current correction.

Fig. 20 Face-to-face test results for reversibility evaluation for R6 (0.06) pair. Blue curve for #6 to #5 and red opposite. Solid curves are voltage-based reversibility tests and dotted curves with current correction. Input current spectra are shown by smooth dashed curves.

Fig. 21 Comparison of R' for PAC F30 (0.3) sensor obtained by Hill-Adams method (red curve) and laser-based direct method (blue curve). Three face-to-face results are given by dashed curves (top three). J' and I_{in} spectra for V103 (1) reference transducer are in green and brown-dash. Transmitter was V192 (1).

Fig. 22 Comparison of R' for PAC R15 (0.15 - in blue) and Fuji Ceramics REF-VL (0.3 - in green) sensors obtained by Hill-Adams method (solid curves) and laser-based direct method (dashed curves).

Fig. 23 Comparison of laser-based sensitivities and Hill-Adams calibration method. Top three curves are for displacement output spectra (T) of three FC500 (2.25) and bottom three represent receiving displacement sensitivities (R). Solid middle curves combine T and R spectra as $(R\ T)^{0.5}$. The dashed curves are $(R\ T)^{0.5}$ from eqn (12) and measured E_{ij} values. (Blue #175; Red #280; Green #281)

Fig. 24 Details of the middle group of curves from Fig. 23. Solid curves are $(R\ T)^{0.5}$ from laser-based direct and indirect methods, dashed curves with eqn (12) and face-to-face tests and dotted curves from TTM. TTM curves were not included in Fig. 23. (Blue #175; Red #280; Green #281)

Appendix

A1. A list of Transducers used in this study

Table A1. Transducers used.

Transducer Model	Manufacturer	Frequency MHz	Aperture size mm	Focusing
V101	Olympus	0.5	25.4	NO
V103	Olympus	1	12.7	NO
V104	Olympus	2.25	25.4	NO
V107	Olympus	5	25.4	NO
V111	Olympus	10	12.7	NO
V189	Olympus	0.5	38	NO
V192	Olympus	1	38	NO
V195	Olympus	2.25	38	NO
R6-alpha	Phys. Acoust.	0.06	12.7	NO
R15	Phys. Acoust.	0.15	12.7	NO
F30-alpha	Phys. Acoust.	0.2-0.7	12.7	NO
FC500	AET Corp	2.25	19	NO
REF-VL	Fuji Ceram.	0.05-0.6	25	NO

A2. Details of home-built current probe

The home-built current probe uses a current transformer with a ferrite bead (#1: 6.30 mm length (L), 3.68 mm outside diameter (OD) and 1.42 mm inside diameter (ID)). The dark-grey colored core material appears to be Material 43 (usually used for 25-300 MHz EMI applications) as this was taken from a PC power supply. The initial permeability measured was 914 vs. specification of 800-850 for Material 43. We also tried other bead sizes. Two more sizes were longer, #2: 9.09 mm L, 3.51 mm OD, 0.71 mm ID, #3: 15.24 mm L, 4.01 mm OD, 1.83 mm ID. Core #2 had the initial permeability of 1694, indicating it is of Material 31. This came from a bead-on-wire unit. Core #3 had a low initial permeability of 427 or Material 44 and it came from an LED power supply. All of them behaved similarly in terms of current waveform for a pulse input. Secondary winding was two turns of 0.13 mm diameter enamel wire, giving nominal current sensitivity of 0.5 V/A with 1-Ω shunt.

For the calibration, the output of the pulser, discussed in Sec. 2.1, was fed to a resistive load of 50 Ω (standard BNC terminator) or a capacitive load of 3.03 or 21.2 nF. For the 50-Ω case, we already have Hioki current probe measurement, as shown in Fig. A1 a). The average of the measured impedance was 34.79 dB (to 10 MHz) or 34.42 dB to 2 MHz (Note 50 Ω corresponds to 34.0 dB). In calibrating our device, the mono-polar pulse was found unsuitable as dc level affected the output, especially at 100 kHz or lower. Thus, we used sinewaves as input and compared the rms values. As expected, the probe sensitivity for #1 ferrite bead decreased at

low frequencies below 200 kHz. Correction factors vs. frequency plot is given in Fig. A1 b). Since the corrected 50-Ω data compared well with the Hioki probe, the capacitive data was not used.

The current sensitivity is shown in Fig. A2 for ferrite beads #1 (used in this study), #2 and #3. The sensitivity is in V/A, but is given in dB scale. All three are within a few tenth of dB to the nominal (theoretical) value of 6 dB and decrease at lower frequency. Of the three, #2 bead provided the best low frequency characteristics, extending the –3-dB point down to 15 kHz. The present results show that a current probe for ultrasonic testing can be built in house using ferrite beads available in laboratory.

Figure Caption

Fig. A1. a) FFT magnitude vs. frequency plots for pulse input signal (– 40 dB: blue curve), same for current from Hioki probe (scale corrected by + 20 dB: red curve) and measured impedance, Z (ohms expressed in dB scale: black curve) vs. frequency,
b) Impedance correction obtained from sinewave calibration vs. frequency. This curve was fitted to $\Delta Z = 8.23 \ln(f) + 34.72$ below 50 kHz and $\Delta Z = 11.74 \exp(-0.028 f)$ above 50 kHz. Here, f is frequency in kHz.

Fig. A2. The current sensitivity (in V/A, but is given in dB scale) for three home-built current probes vs. frequency. #1 ferrite bead: Red curve, #2, Blue curve, #3, Green curve.

Figures with Caption Rev2

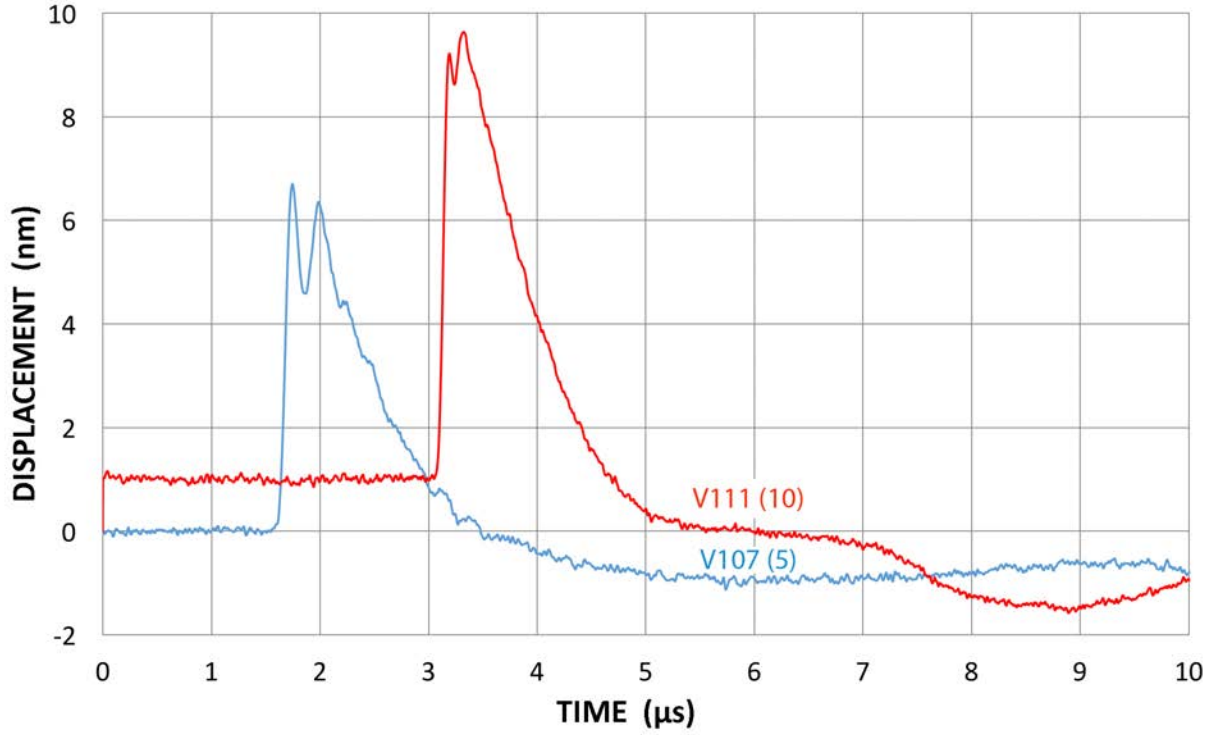

Fig. 1-a Displacement output of transducers, V107 and V111.

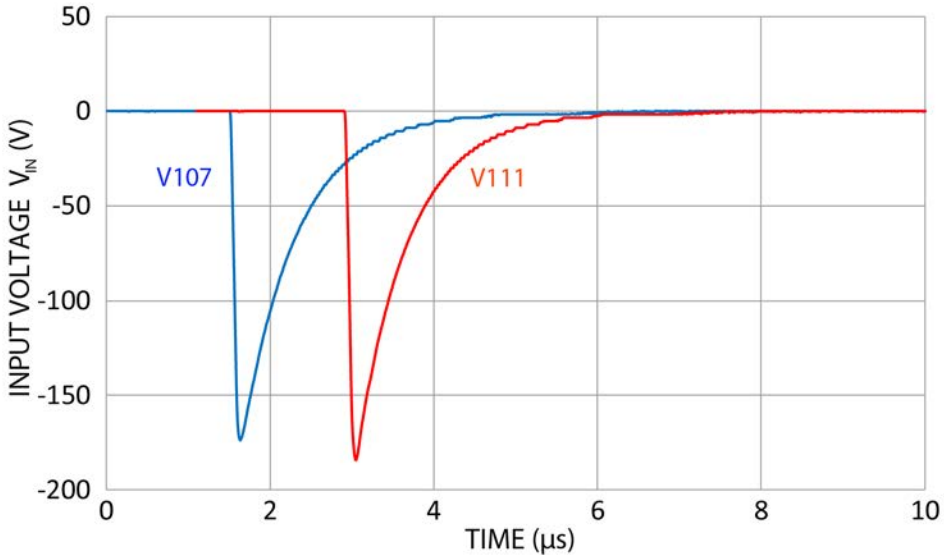

Fig. 1-b Waveforms of pulse input (V_{in} in V) with transducer connected.

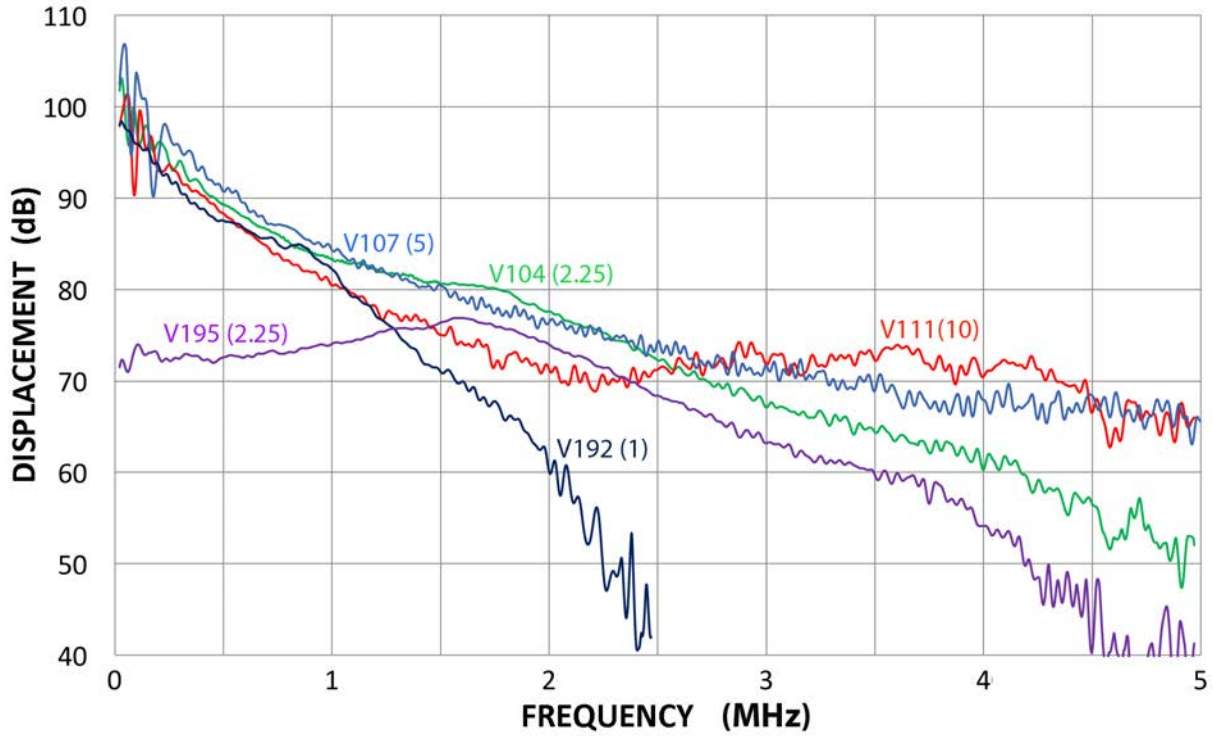

Fig. 2 Displacement output spectra for five transducers (V104, V107, V111, V192 and V195) in reference to 0 dB at 1 nm.

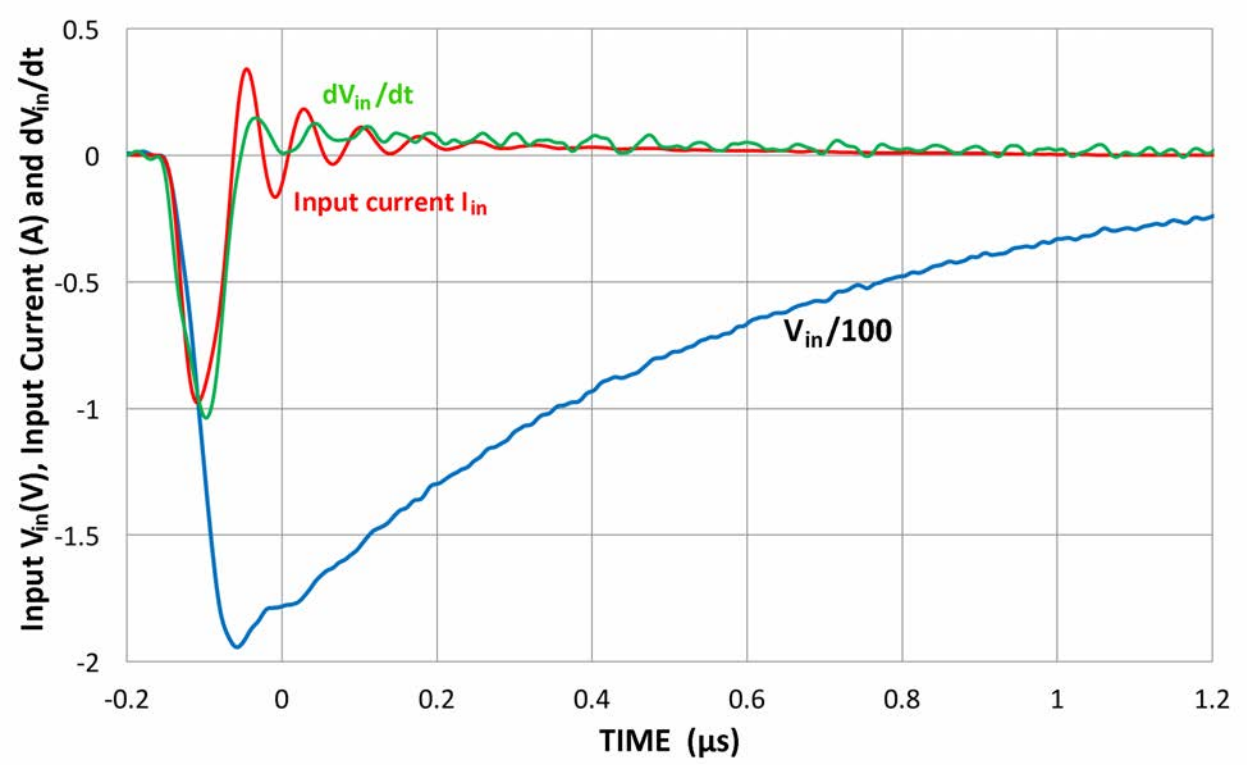

Fig. 3 Waveforms of pulse input (V_{in}/100 in V), current input (I_{in} in A), dV_{in}/dt (peak matched to I_{in}) for R15 transducer.

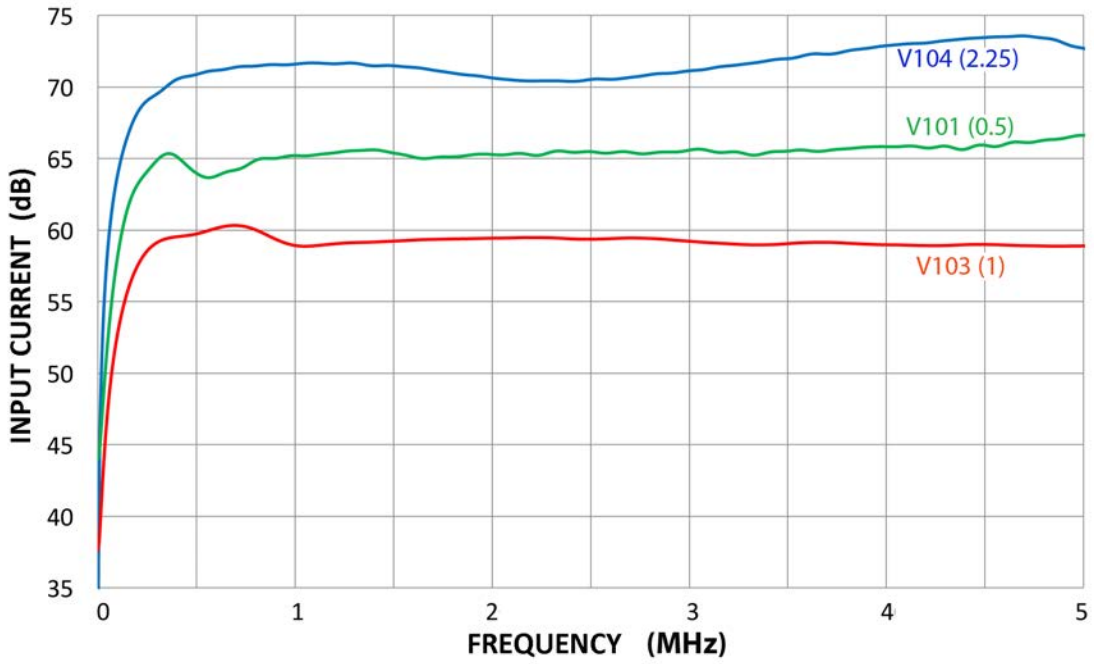

Fig. 4 Input current spectra for V101, V103 and V104 transducers in reference to 0 dB at 1 A.

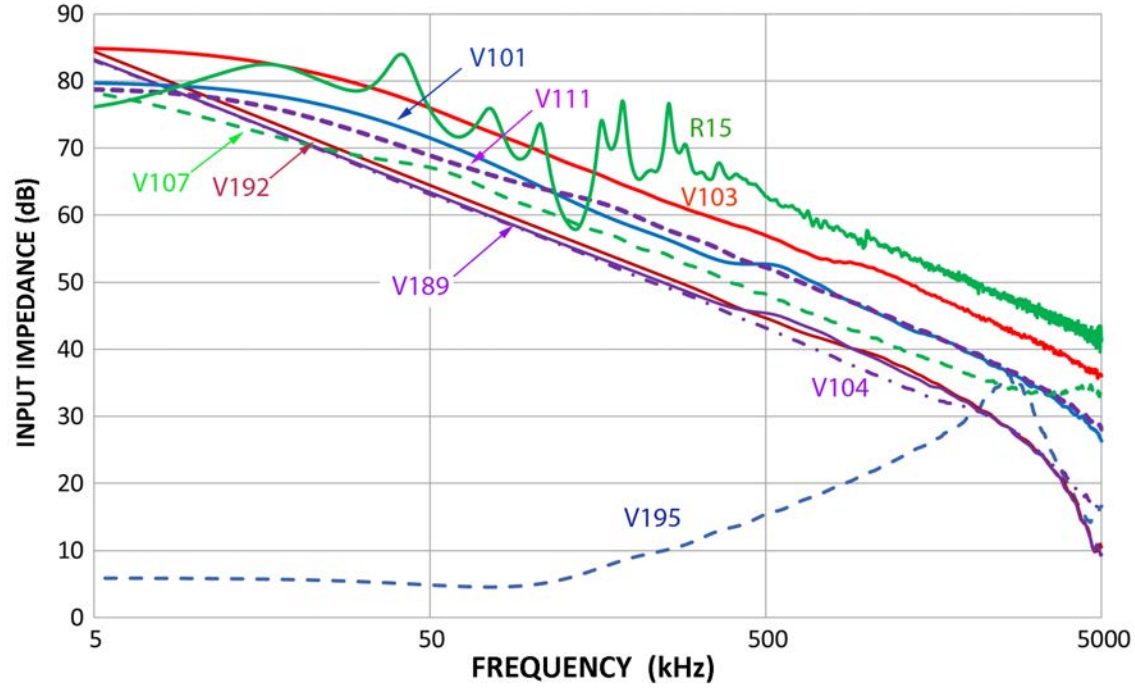

Fig. 5 Input electrical impedance for nine transducers in reference to 0 dB at 1 ohm. From top, R15 (green – 0.15), V103 (red - 1), V101 (blue – 0.5), V111 (purple dash - 10), V107 (green dash - 5), V192 (dark red - 1), V189 (purple - 0.5), V104 (purple dash-dot – 2.25), and V195 (blue dash – 2.25).

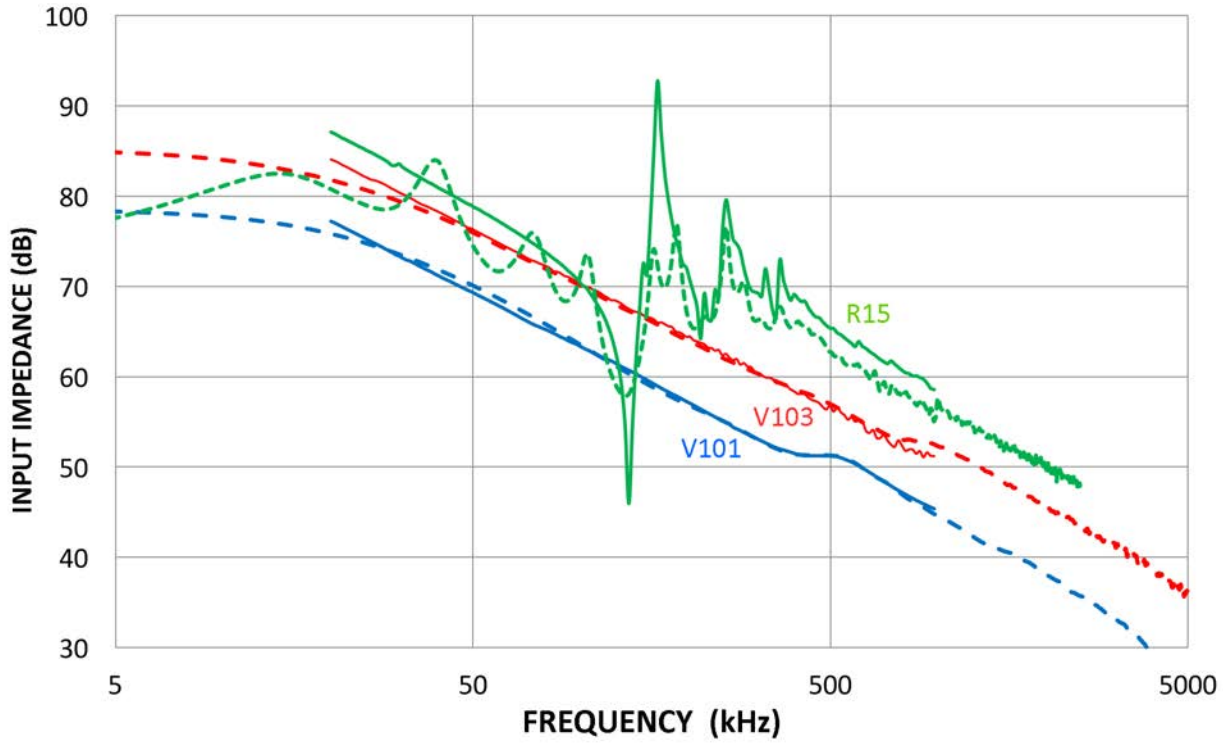

Fig. 6 Input electrical impedance in dB for three transducers, R15 (0.15), V103 (1) and V101 (0.5). Static Z in solid curves and dynamic Z in dashed curves.

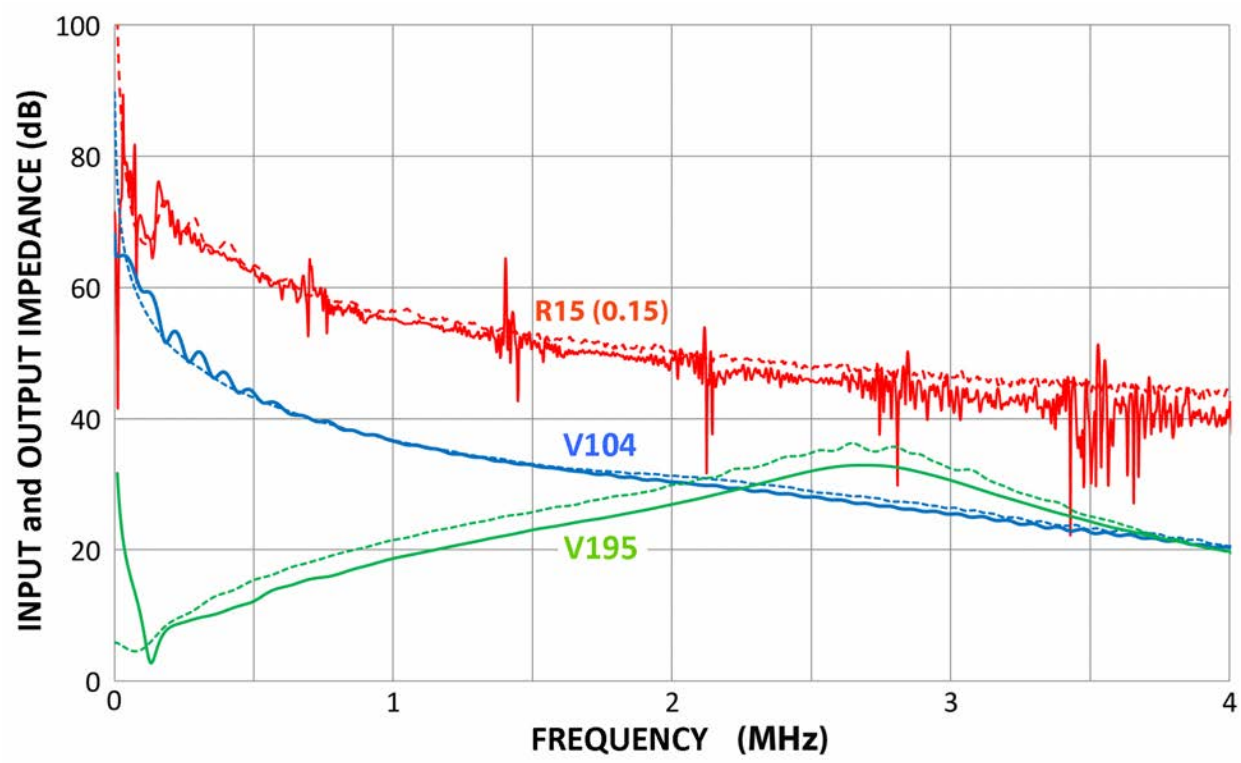

Fig. 7 Input and output electrical impedance in dB for three transducers, R15, V104 (2.25) and V195 (2.25). Output Z in solid curves and input Z in dashed curves.

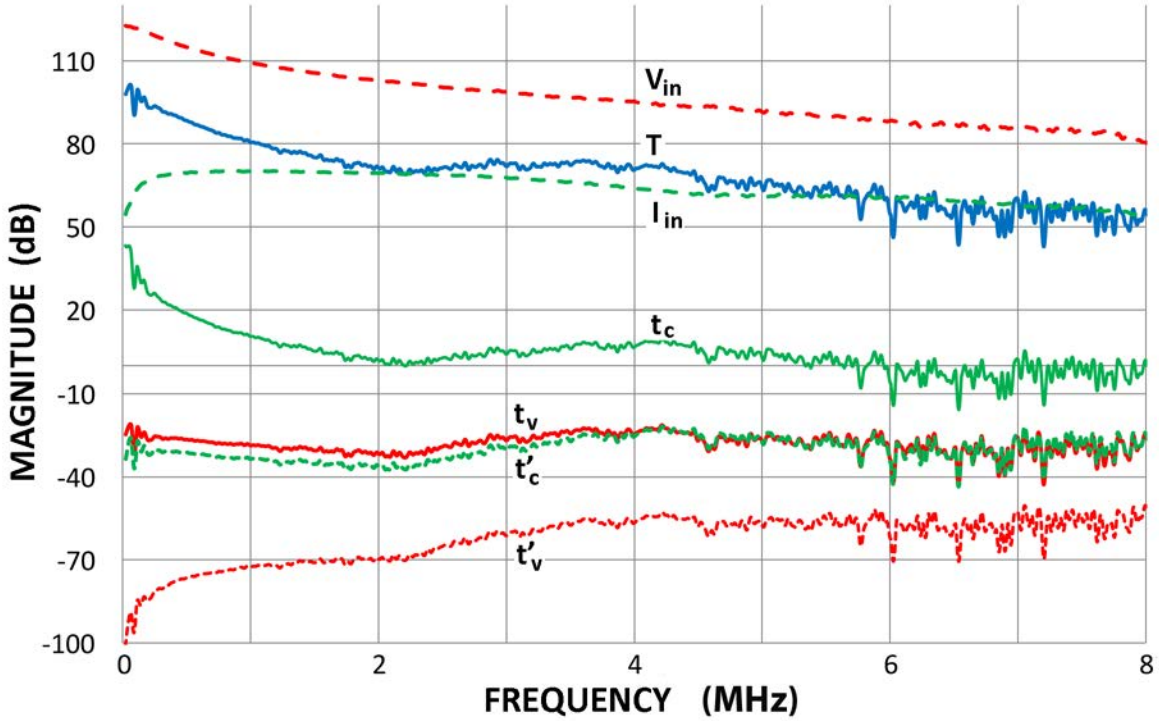

Fig. 8 Four types of transmission sensitivities (see text for definitions) for V107 (5) together with pulse voltage spectrum (V_{in}), input current spectrum (I_{in}) and displacement spectrum (T).

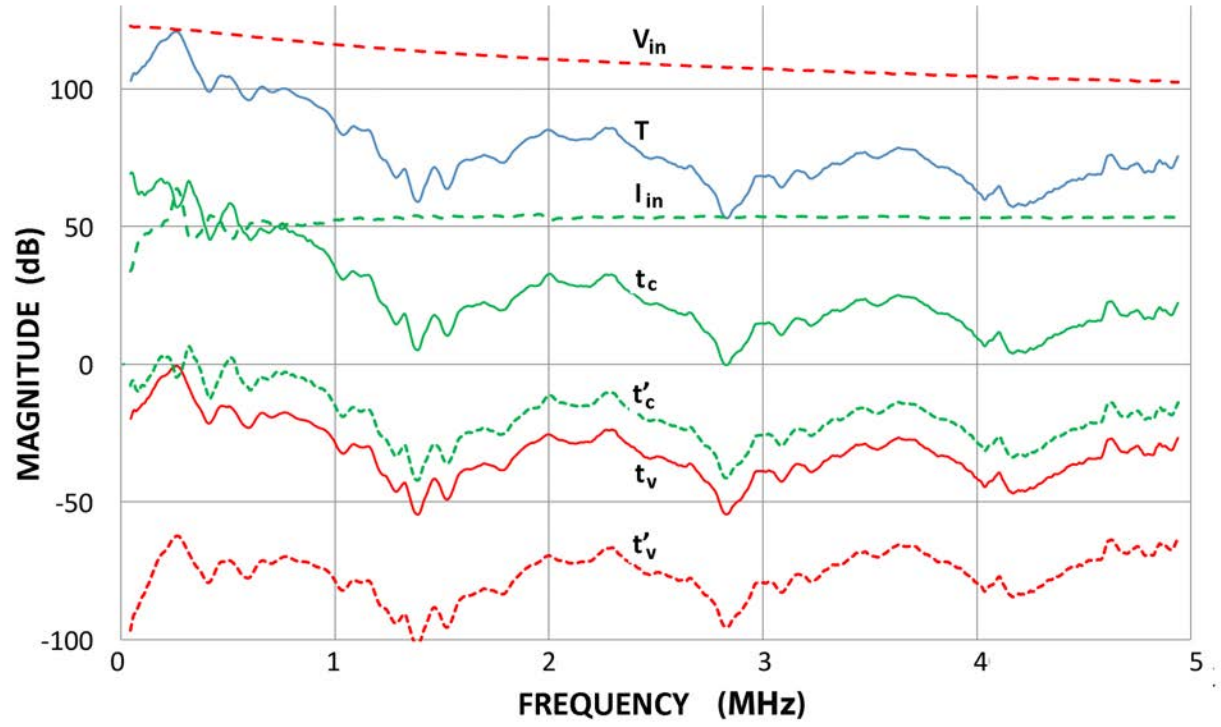

Fig. 9 Four types of transmission sensitivities (see text for definitions) for R15 (0.15) together with pulse voltage spectrum (V_{in}), input current spectrum (I_{in}) and displacement spectrum (T).

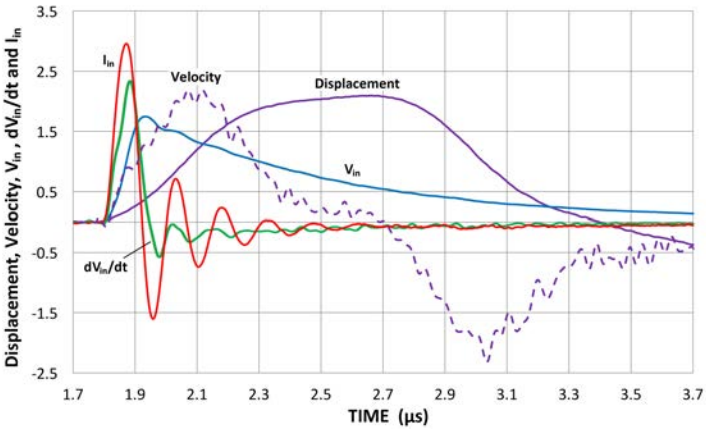

Fig. 10-a Waveforms of displacement and velocity output of V101 (0.5) transducer with input pulse (V_{in}/100 in V), input current (A) and dV_{in}/dt. Displacement is divided by 5 and in nm. The velocity and dV_{in}/dt are scaled to be comparable to the peaks of other waveforms.

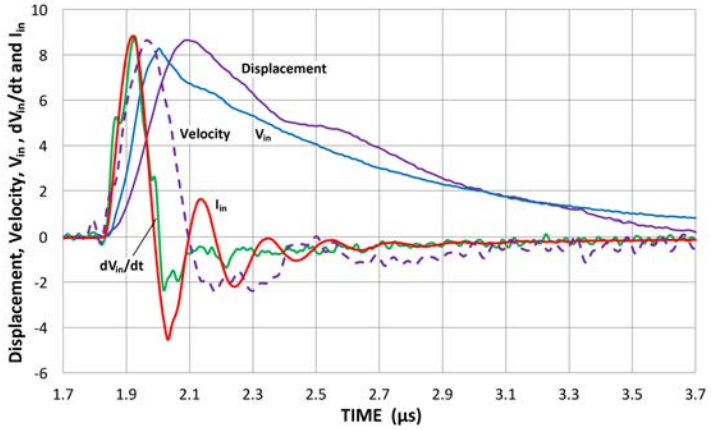

Fig. 10-b Waveforms of displacement and velocity output of V104 (2.25) transducer with input pulse (V_{in}/100 in V), twice input current (in A) and dV_{in}/dt. Displacement is in nm. The velocity and dV_{in}/dt are scaled to be comparable to the peaks of other waveforms.

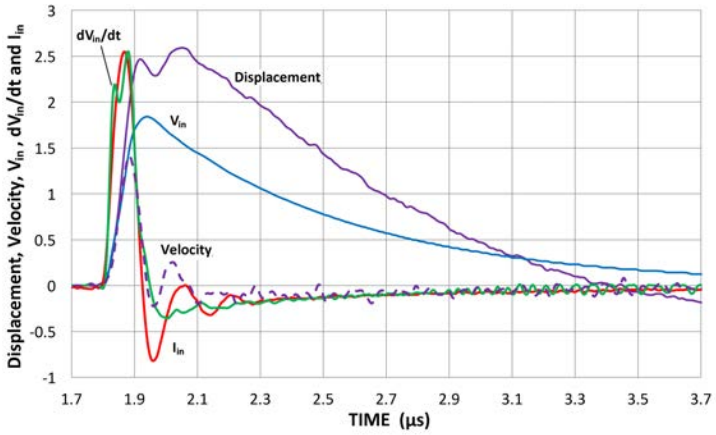

Fig. 10-c Waveforms of displacement and velocity output of V111 (10) transducer with input pulse (V_{in}/100 in V), I_{in} (in A) and dV_{in}/dt. Displacement in nm is divided by 3. The velocity and dV_{in}/dt are scaled to be comparable to the peaks of other waveforms.

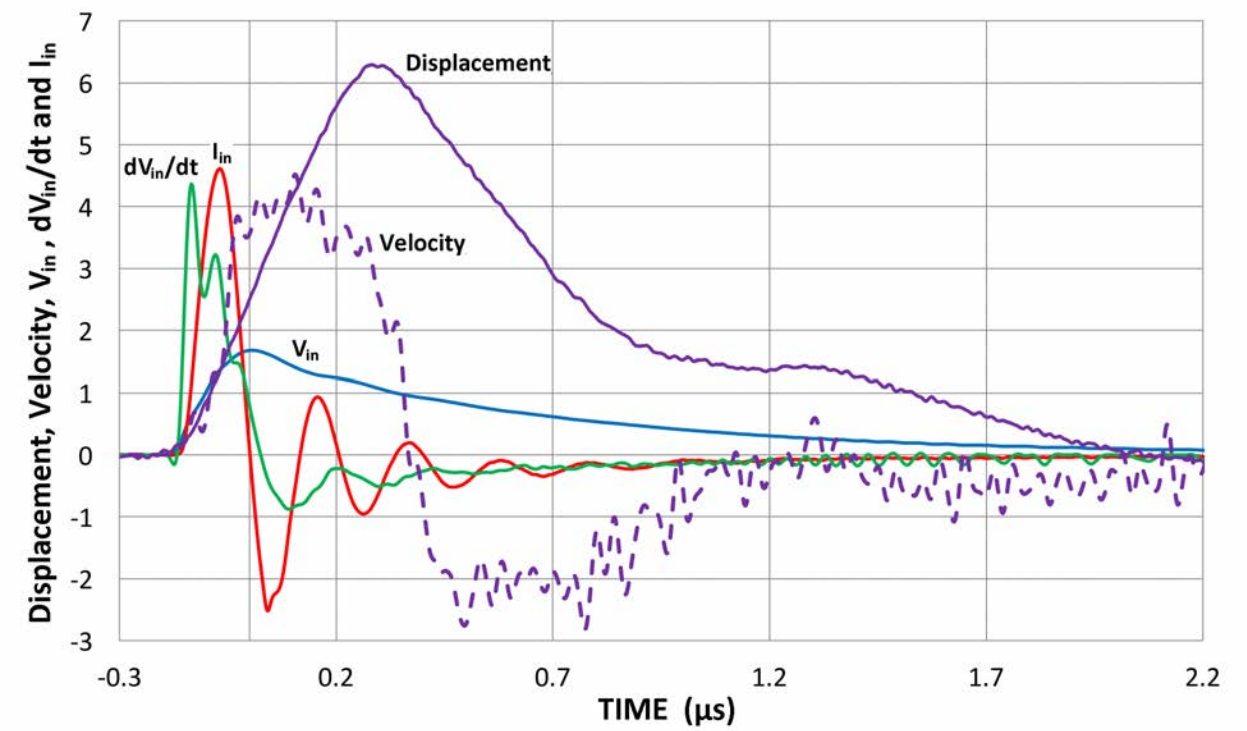

Fig. 11 Waveforms of displacement and velocity output of V192 (1) transducer with input pulse (V_{in}/100 in V), I_{in} (in A) and dV_{in}/dt. Displacement is in nm. The velocity and dV_{in}/dt are scaled to be comparable to the peaks of other waveforms.

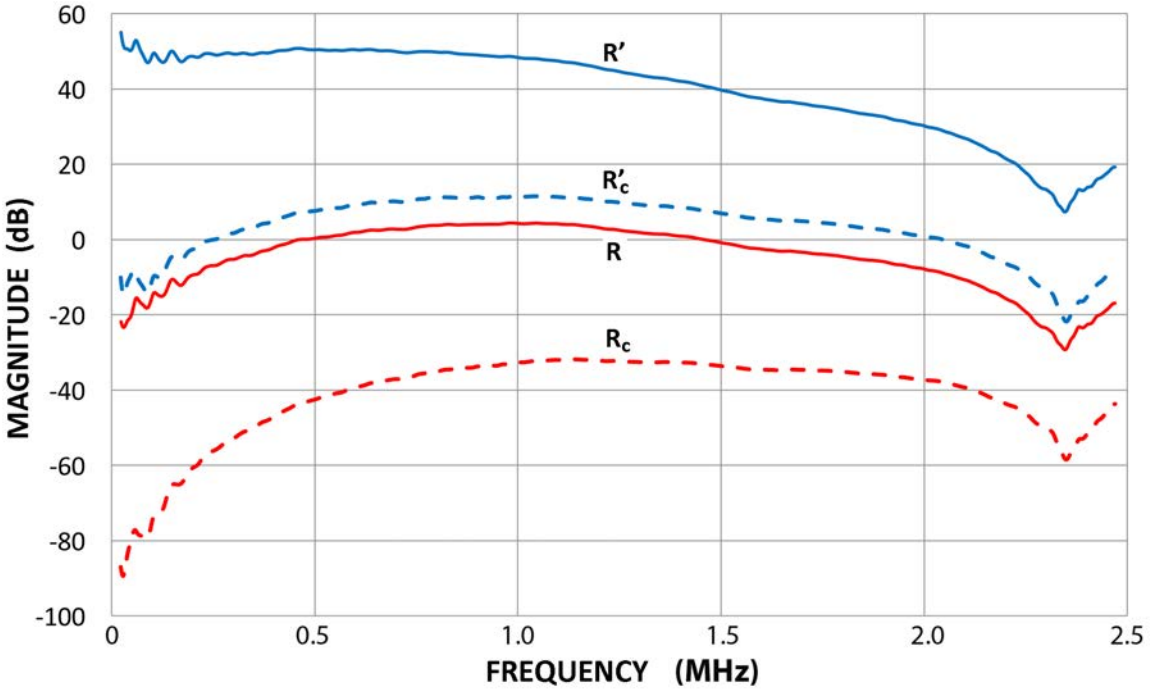

Fig. 12-a Receiving sensitivities of V192 (1) transducer. See text for definitions of symbols.

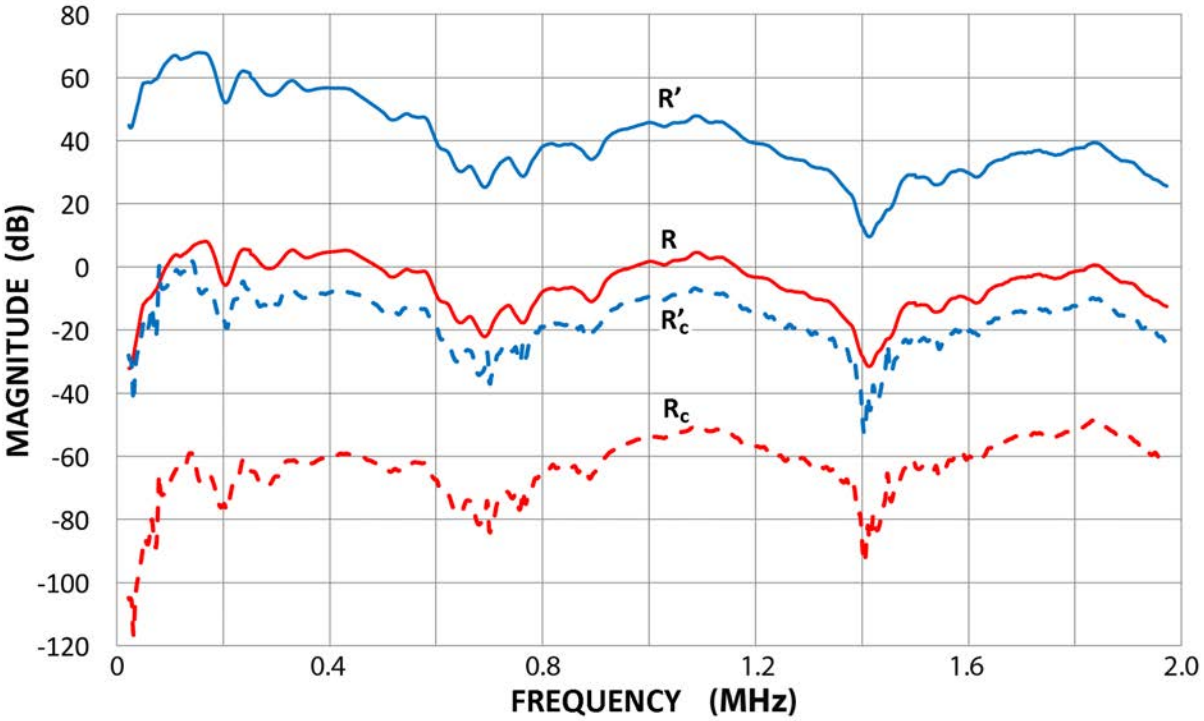

Fig. 12-b Receiving sensitivities of R15 (0.15) transducer. See text for definitions of symbols.

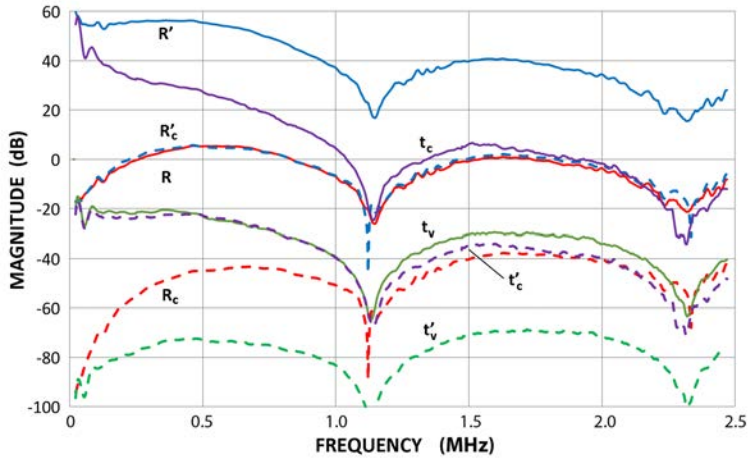

Fig. 13-a Four types of transmission sensitivities and four types of receiving sensitivities of V101 (1) transducer.

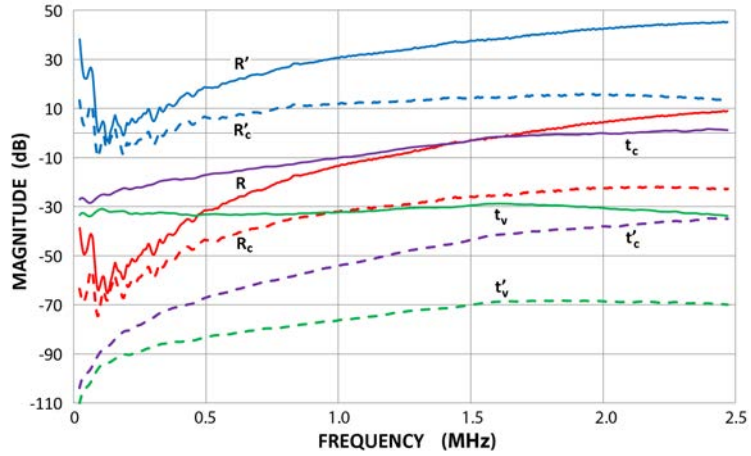

Fig. 13-b Four types of transmission sensitivities and four types of receiving sensitivities of V195 (2.25) transducer.

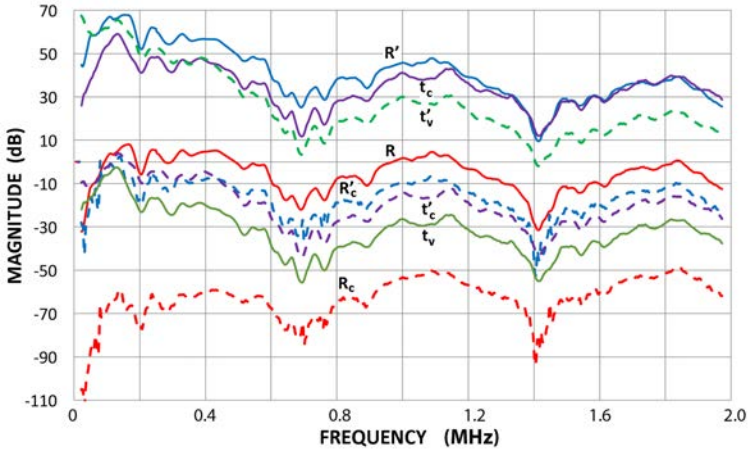

Fig. 13-c Four types of transmission sensitivities and four types of receiving sensitivities of R15 (0.15) transducer.

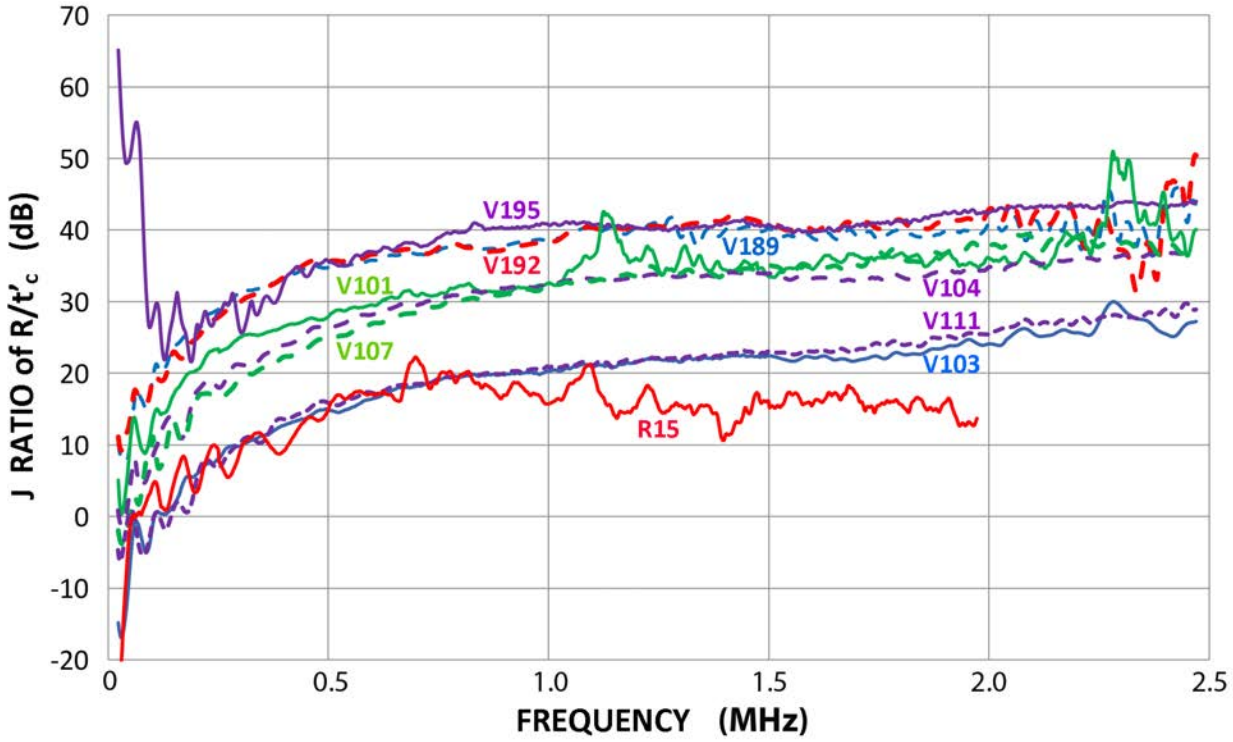

Fig. 14 J ratios of R/t'_c in dB for nine transducers. From top: V195 (purple – 2.25), V189 (blue dash - 0.5), V192 (red dash - 1), V101 (green - 0.5), V104 (purple dash – 2.25), V107 (green dash - 5), V111 (purple dash - 10), V103 (blue - 1), R15 (red – 0.15).

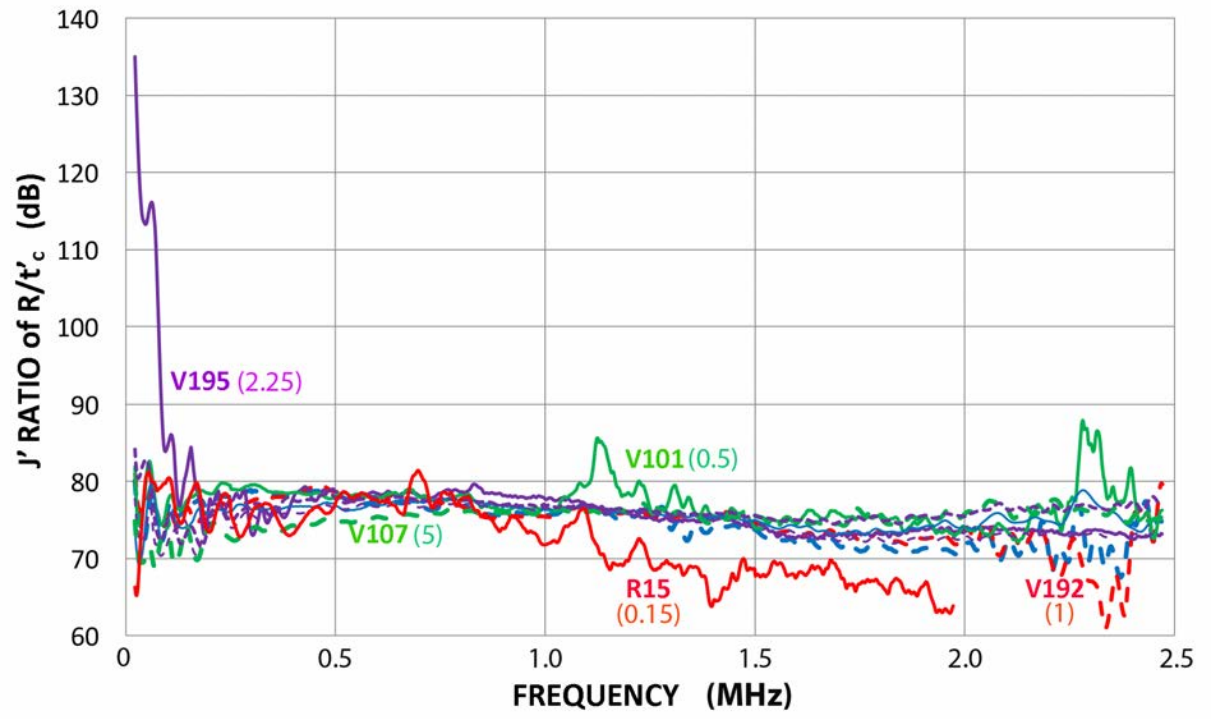

Fig. 15 J' ratios of R'/t'_c in dB for nine transducers. Same color code used as in Fig. 14.

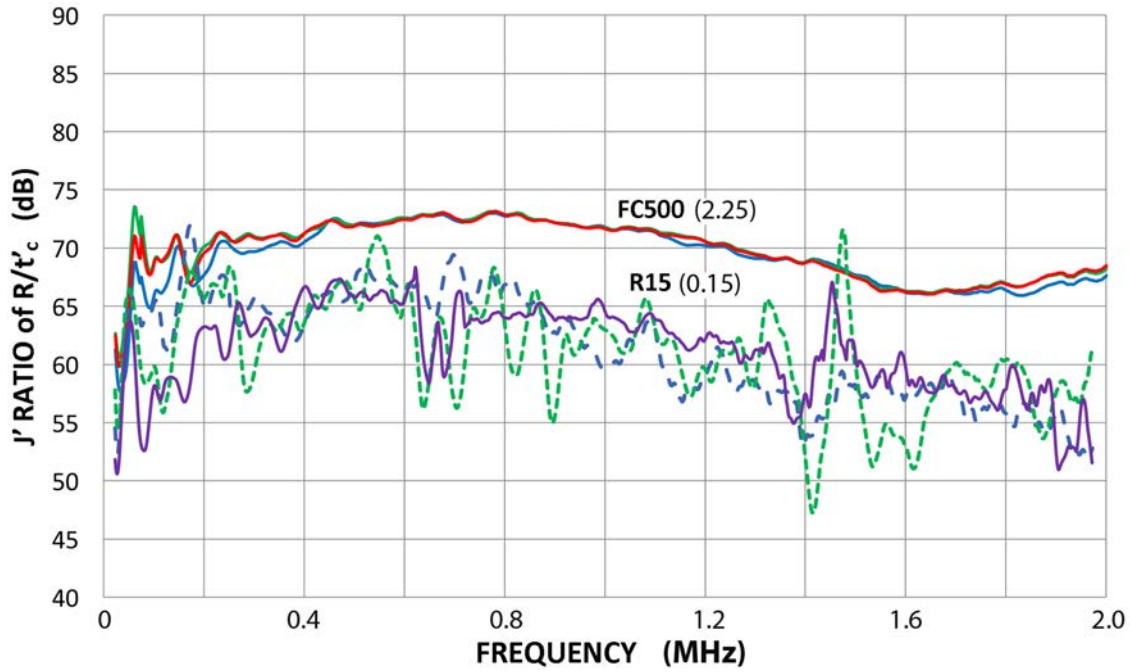

Fig. 16 J' ratios of R'/t'_c in dB for three FC500 (2.25) and three R15 (0.15) transducers. Additions of 5 dB for FC500 and 12 dB for R15 are needed to make J' values equivalent to nominal 25 mm diameter used in Fig. 14.

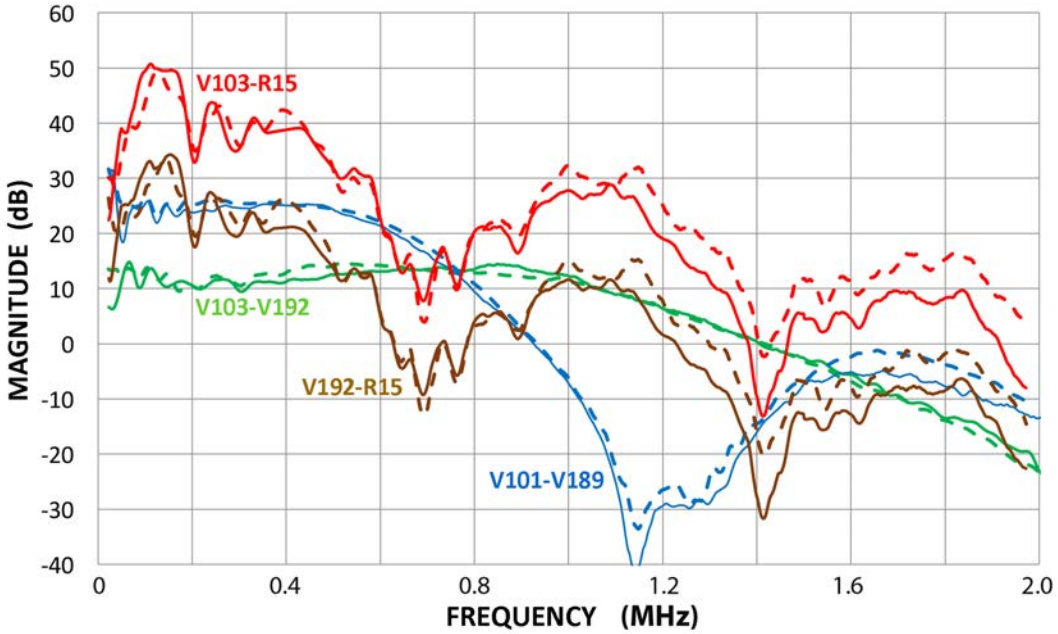

Fig. 17 Face-to-face test results for reversibility evaluation. Solid curves are for the combination of V103 (1) to R15 (0.15) (red), V103 (1) to V192 (1) (green), V192 (1) to R15 (0.15) (brown) and V101 (0.5) to V189 (0.5) (blue). Dashed curves are for the opposite signal direction.

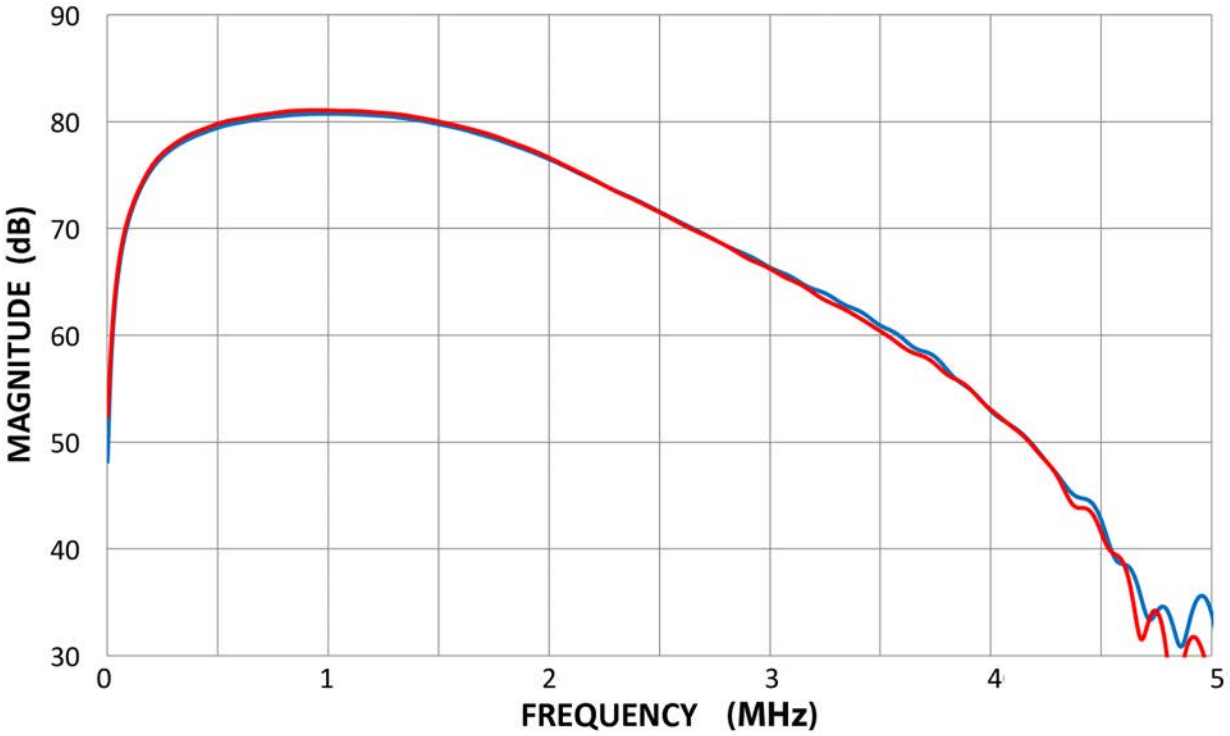

Fig. 18 Face-to-face test results for reversibility evaluation for FC500 (2.25) pair. Blue curve for #280 to #281 and red opposite.

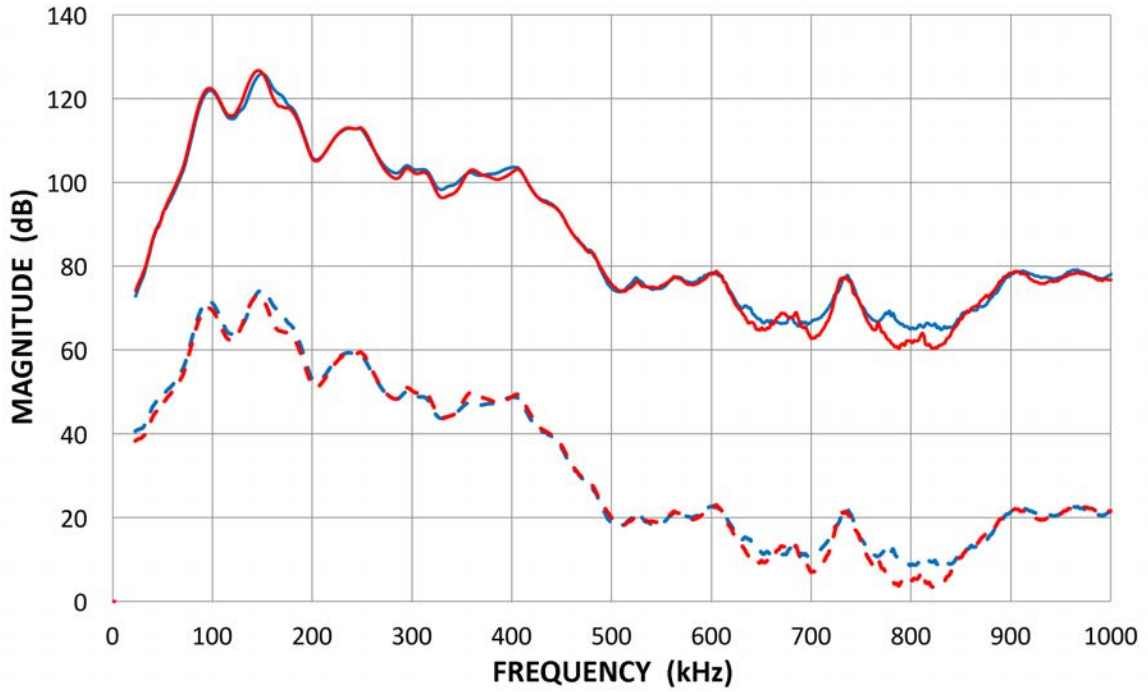

Fig. 19 Face-to-face test results for reversibility evaluation for R15 (0.15) pair. Blue curve for #67 to #90 and red opposite. Solid curves are voltage-based reversibility tests and dashed curves with current correction.

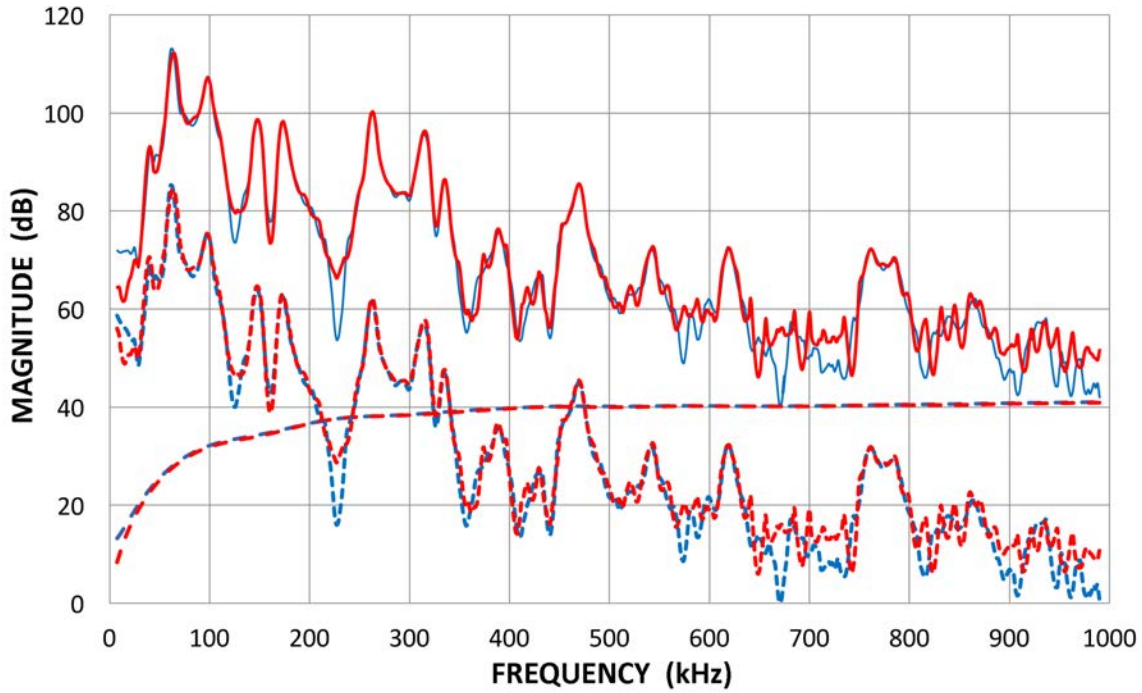

Fig. 20 Face-to-face test results for reversibility evaluation for R6 (0.06) pair. Blue curve for #6 to #5 and red opposite. Solid curves are voltage-based reversibility tests and dotted curves with current correction. Input current spectra are shown by smooth dashed curves.

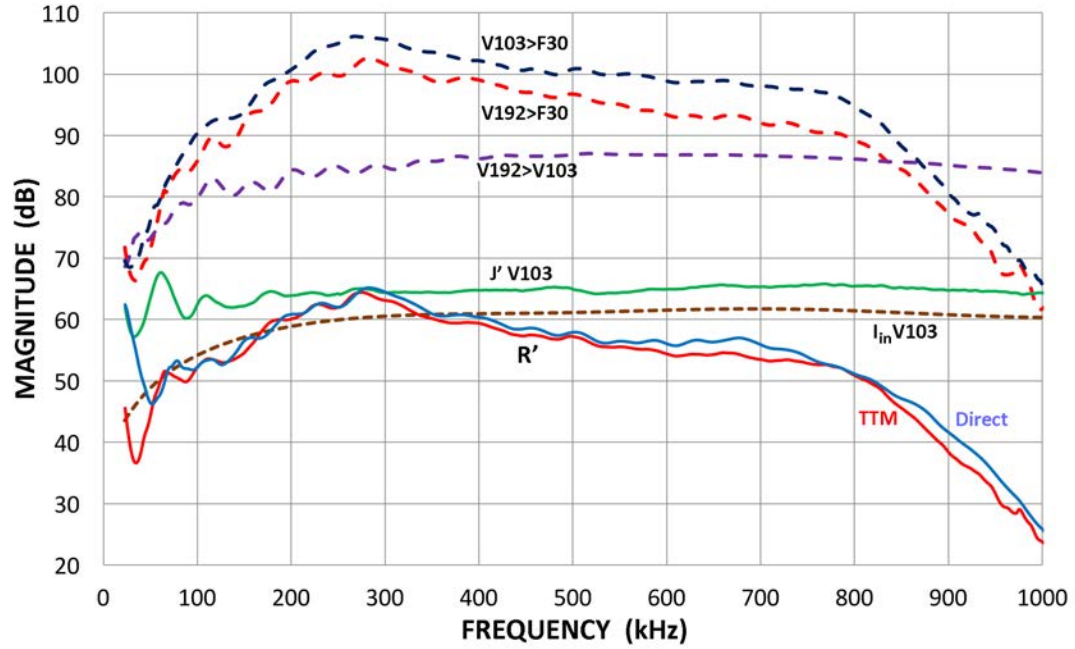

Fig. 21 Comparison of R' for PAC F30 (0.3) sensor obtained by Hill-Adams method (red curve) and laser-based direct method (blue curve). Three face-to-face results are given by dashed curves (top three). J' and I_{in} spectra for V103 (1) reference transducer are in green and brown-dash. Transmitter was V192 (1).

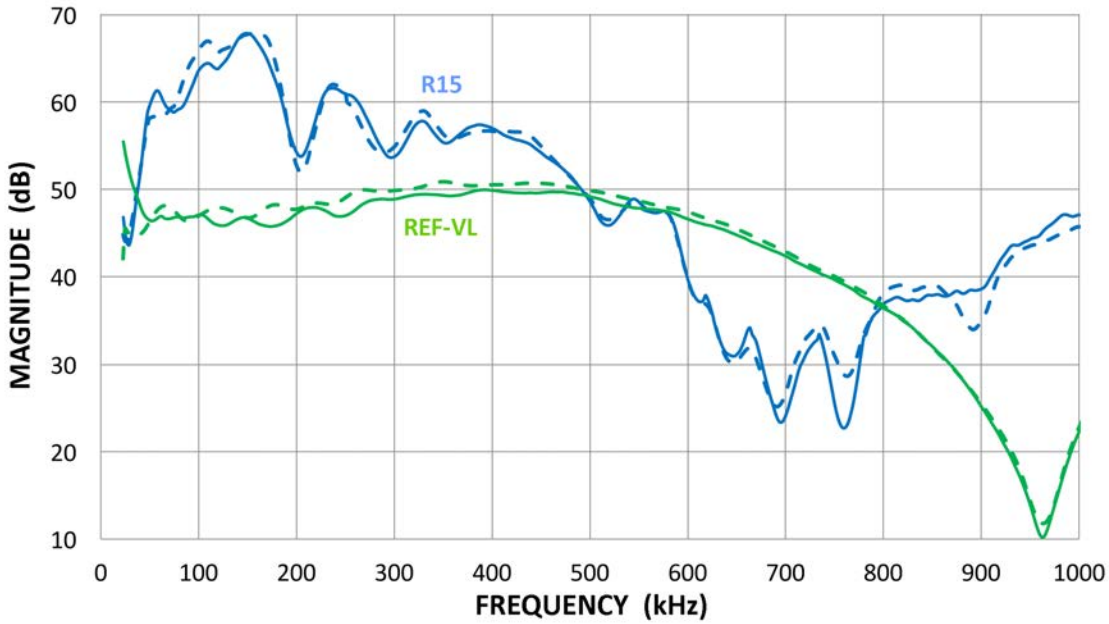

Fig. 22 Comparison of R' for PAC R15 (0.15 - in blue) and Fuji Ceramics REF-VL (0.3 - in green) sensors obtained by Hill-Adams method (solid curves) and laser-based direct method (dashed curves).

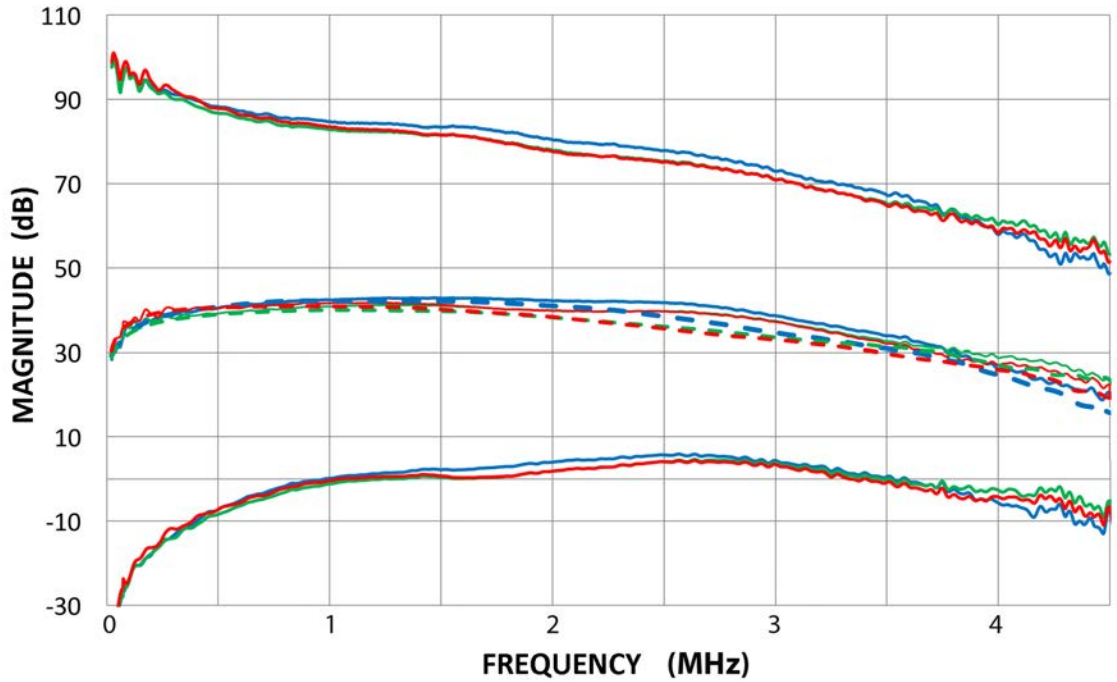

Fig. 23 Comparison of laser-based sensitivities and Hill-Adams calibration method. Top three curves are for displacement output spectra (T) of three FC500 (2.25) and bottom three represent receiving displacement sensitivities (R). Solid middle curves combine T and R spectra as $(R\,T)^{0.5}$. The dashed curves are $(R\,T)^{0.5}$ from eqn (12) and measured E_{ij} values. (Blue #175; Red #280; Green #281)

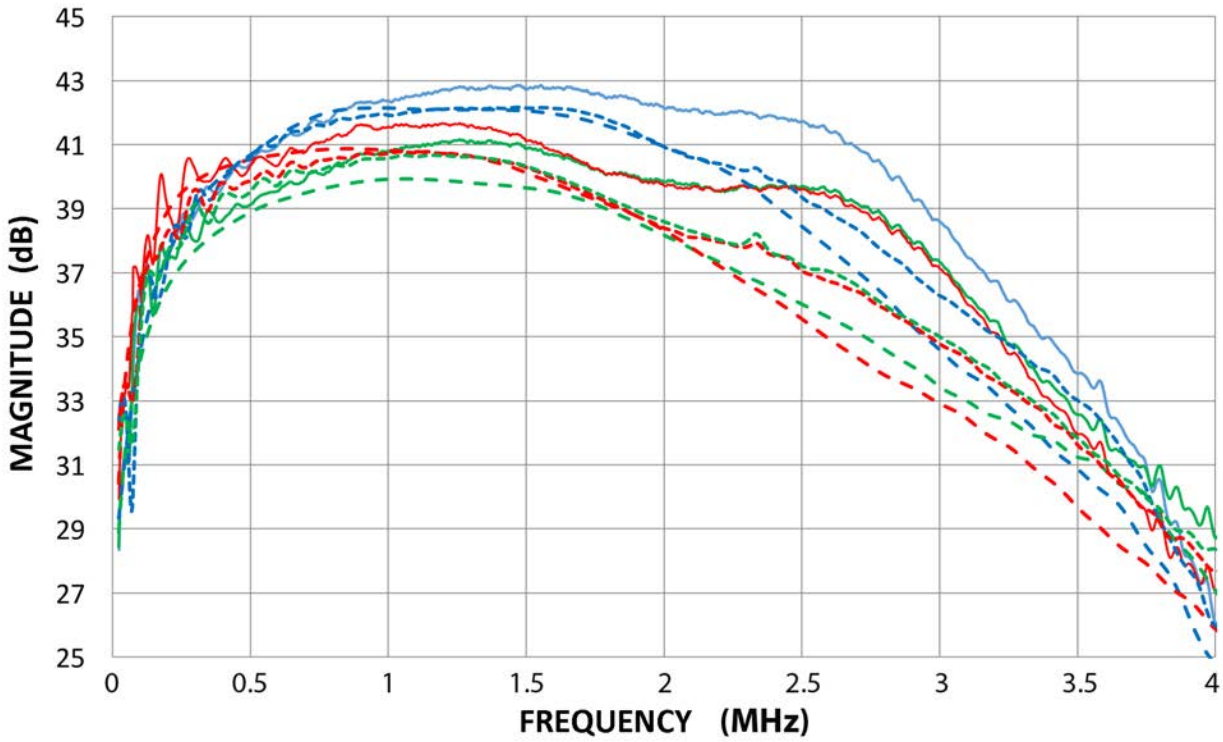

Fig. 24 Details of the middle group of curves from Fig. 23. Solid curves are $(R\,T)^{0.5}$ from laser-based direct and indirect methods, dashed curves with eqn (12) and face-to-face tests and dotted curves from TTM. TTM curves were not included in Fig. 23. (Blue #175; Red #280; Green #281)

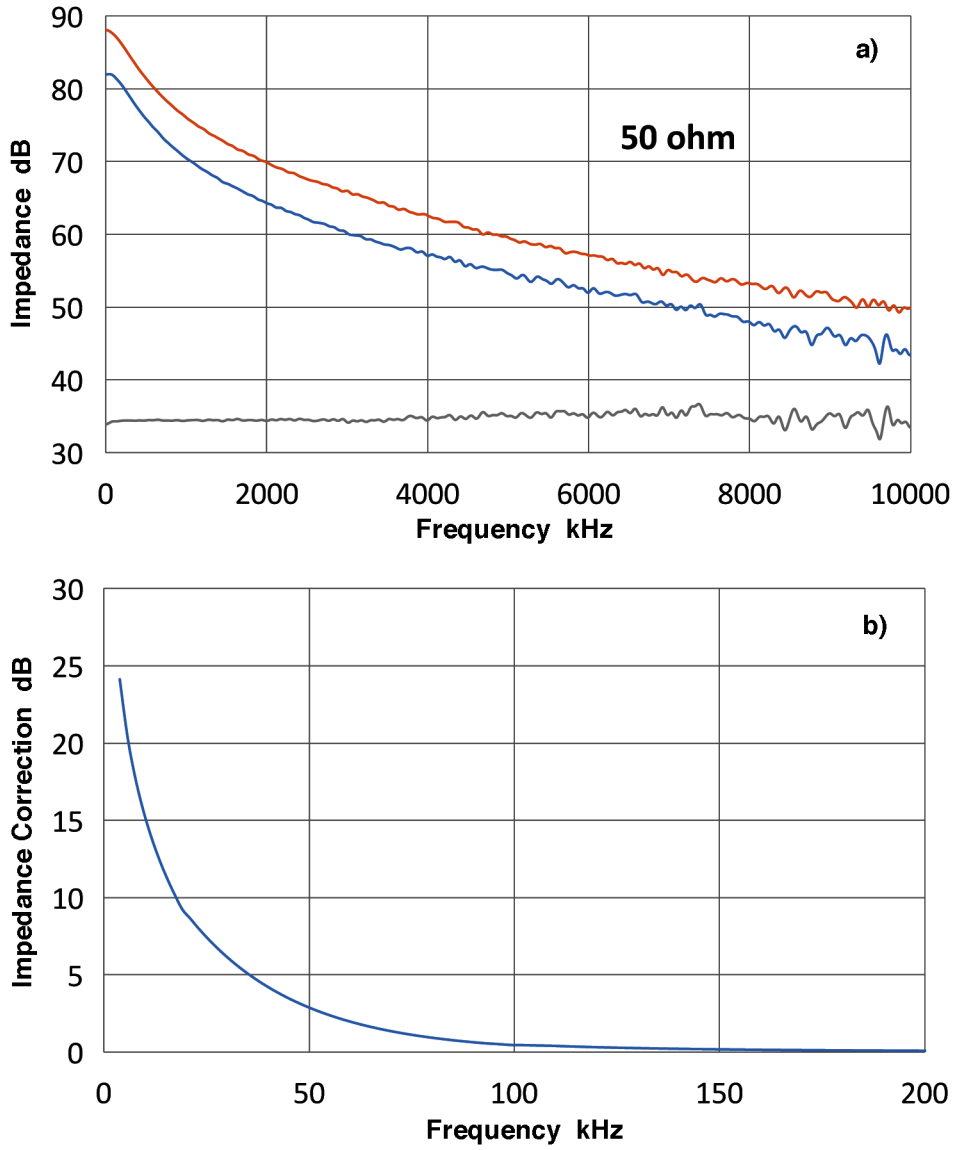

Fig. A1. a) FFT magnitude vs. frequency plots for pulse input signal (– 40 dB: blue curve), same for current from Hioki probe (scale corrected by + 20 dB: red curve) and measured impedance, Z (ohms expressed in dB scale: black curve) vs. frequency.
b) Impedance correction obtained from sinewave calibration vs. frequency. This curve was fitted to $\Delta Z = 8.23 \ln(f) + 34.72$ below 50 kHz and $\Delta Z = 11.74 \exp(-0.028 f)$ above 50 kHz. Here, f is frequency in kHz.

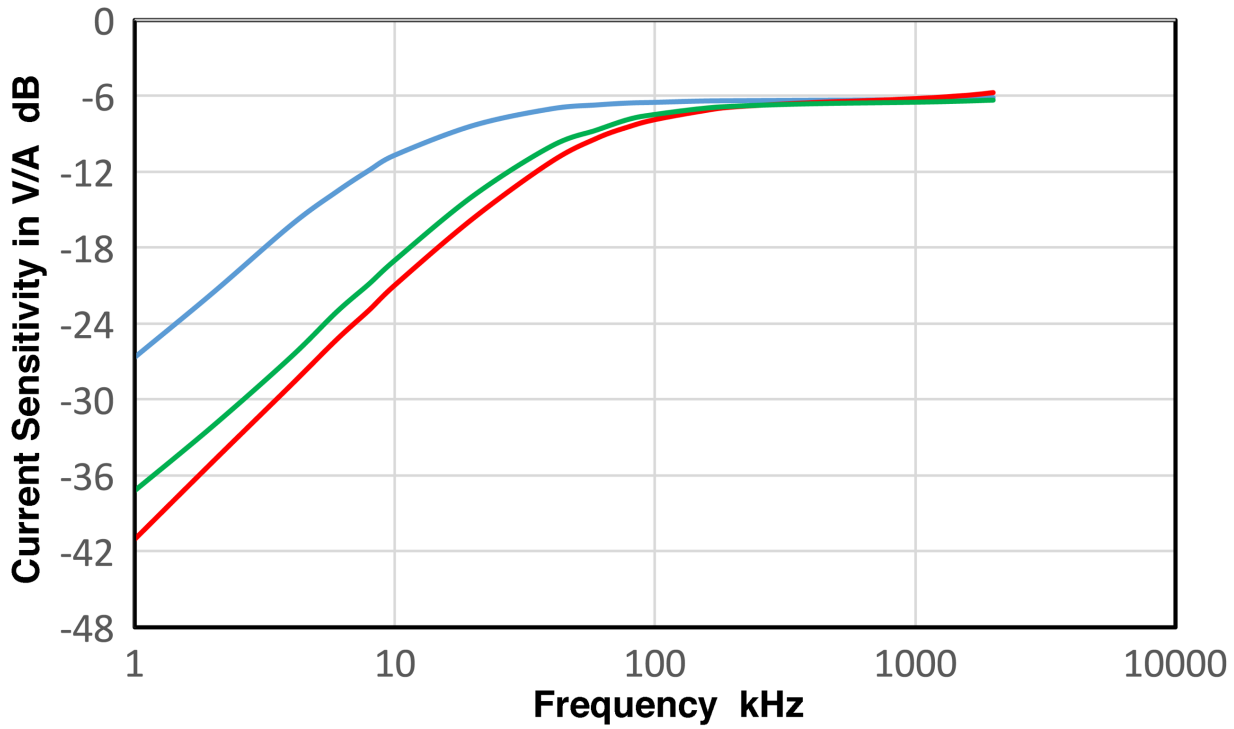

Fig. A2. The current sensitivity (in V/A, but is given in dB scale) for three home-built current probes vs. frequency. #1 ferrite bead: Red curve, #2, Blue curve, #3, Green curve.